

Modeling of High-Pressure Entrained-Flow Char Oxidation

Daniel Gundersen

A thesis submitted to the faculty of
Brigham Young University
in partial fulfillment of the requirements for the degree of

Master of Science

Thomas H. Fletcher, Chair
Andrew R. Fry
Morris D. Argyle

Department of Chemical Engineering
Brigham Young University

Copyright © 2022 Daniel Gundersen

All Rights Reserved

ABSTRACT

Modeling of High-Pressure Entrained-Flow Char Oxidation

Daniel Gundersen
Department of Chemical Engineering, BYU
Master of Science

Coal plays a significant role in electricity production worldwide and will into the foreseeable future. Technologies that improve efficiency and lower emissions are becoming more popular. High pressure reactors and oxyfuel combustion can offer these benefits. Designing new reactors effectively requires accurate single particle modeling.

This work models a high-pressure, high-temperature, high-heating rate, entrained-flow, char oxidation data set to generate kinetic parameters. Different modeling methods were explored and a sensitivity analysis on char burnout was performed by varying parameters such as total pressure, O₂ partial pressure, O₂ and CO₂ mole fractions, gas temperature, diameter, and pre-exponential factor.

Pressure effects on char burnout modeling were found to be dependent on the set of kinetic parameters chosen. Using kinetic parameters from Hurt-Calo (2001) as opposed to values obtained from Niksa-Hurt (2003) yielded a trend seen in real data sets, that reaction order changes with temperature. Varying O₂ mole fraction and partial pressure showed the most significant changes in char burnout. Varying diameter, total pressure, the pre-exponential factor, CO₂ environment, and gas temperature all changed the char burnout extent as well. The effect of changing those parameters decreases in the order they are listed. Increasing any of these parameters resulted in an increase in char burnout except for particle diameter and CO₂ mole fraction which led to a decrease. Char formation pressure affects reactivity, and a peak in reactivity is shown in this work at the 6 atm condition.

Keywords: char oxidation modeling, high pressure, sensitivity analysis

ACKNOWLEDGEMENTS

I would like to express my appreciation and support to all who have helped me complete my thesis. First, I would like to acknowledge my advisor Dr. Thomas H. Fletcher for all his guiding support and assistance and also his patience and flexibility with me completing this in off hours while I work a full-time job at an oil refinery. This would have been impossible without his influence.

I'd also like to express appreciation for all others involved in assisting with the completion of this project. Thanks to my committee members, Dr. Andrew R. Fry and Dr. Morris D. Argyle, to Troy Holland for helping me learn the CCK code and to Dong Zeng for his assistance in helping find information about his data set. I'd also like to thank the undergraduates who helped in the atmospheric flat flame burner lab, Samantha Schachterle, Shawn Fogleman, and Colson Johnson.

This material is based on work partially supported in part by the Department of Energy, National Nuclear Security Administration, under Award Number DE-NA0002375. I'd like to thank the DOE and specifically the PSAAP project for the funding and connections to have a graduate internship at Lawrence Livermore National Laboratory.

Finally, I'd like to thank my wonderful wife Natalie for all of her support and patience through this project. I could not have completed this without the many sacrifices that she's made on nights and weekends for me to be able to complete this thesis.

TABLE OF CONTENTS

1. Introduction	1
2. Literature Review	3
2.1 Coal	3
2.2 Coal Conversion	3
2.3 Coal Conversion Modeling History	4
2.4 Oxy-Coal Combustion Modeling	5
2.5 High Pressure Char Oxidation Data Sets	7
2.6 Swelling and Annealing	10
2.7 Char Formed at Pressure	12
2.8 Surface Kinetics	14
2.9 Summary	14
3. Objective and Tasks	15
Task 1. Complete the DZ Data Set by Determining Residence Time	16
Task 2. Model the DZ High Pressure High Heating Rate Data Set	16
Task 3. Perform a Sensitivity Analysis with the CCK Code	17
Task 4. Atmospheric FFB Experiments	17
4. High Pressure Modeling Approach	20
4.1 Uniqueness of the DZ Data Set	20
4.1.1 Incomplete Data Set	21
4.1.2 Solving for Residence Time	21
4.2 CCK Code	24
4.2.1 Subroutine Descriptions	25
4.2.2 Effects of Pressure in the CCK Code	25
4.3 Kinetic Considerations	27
4.4 χ Factor Challenges with CCK	32
4.4.1 χ Factor and Combustion Zones	32
4.4.2 CCK Diffusion Limitations	34
5. Results and Discussion	37
5.1 Modeling Conditions	37
5.2 Solving for the Pre-Exponential Factor	41
5.3 Comparison with Char Burnout Data	42

5.3.1	2.5 atm Case	43
5.3.2	6 atm Case	44
5.3.3	10 atm Case	46
5.3.4	Group Solve.....	47
5.3.5	Statistical Comparison.....	49
5.3.6	Summary.....	52
5.4	Sensitivity Analysis.....	54
5.4.1	Total Pressure and O ₂ Partial Pressure	55
5.4.2	CO ₂ Gas Composition	61
5.4.3	Gas Temperature.....	62
5.4.4	Diameter	63
5.4.5	Pre-exponential Factor.....	64
5.4.6	Summary.....	65
6.	Summary and Conclusions	66
7.	Recommendations.....	69
	References:.....	71
	Appendix A: CCK Code.....	75
	Appendix B: Atmospheric Flat Flame Burner Data.....	76
	Appendix C: Additional Data	78

LIST OF TABLES

Table 2-1 Recent Coal Conversion Modeling History 5
Table 2-2: High Pressure Combustion Data Sets..... 7
Table 4-1: Recreated Residence Times for the Large Pitt 8 Coal Sampling Locations 24
Table 4-2: Kinetic Parameters: Niksa-Hurt and Hurt-Calo 29
Table 5-1: Data Set Gas Temperature Profiles 38
Table 5-2: Data Set Velocity Profiles 38
Table 5-3: Data Set Feed Gas Rates and Product Compositions 39
Table 5-4: Data Set Residence Times and Collection Probe Heights* 40
Table 5-5: Data Set Diameter, Heating Rate, and Mode of Burning..... 40
Table 5-6 Data Set Proximate and Ultimate Analysis-Pitt8 40
Table 5-7: Data Set Char Burnout Data for each O₂ condition..... 41
Table 5-8: Various Model Comparison Data..... 50
Table 5-9: Pre-exponential Factors from Modeling..... 52
Table 5-10: Sensitivity Analysis Parameter Base Case and Range 54
Table 5-11: Legend explanation for Figures 5-13 and 5-14 58
Table 5-12: Sensitivity Analysis Results 65
Table C-1: Various Model Comparison Data (Group Solutions) 78
Table C-2: Various Model Comparison Data (Single Point Solutions)..... 79
Table C-3: Pre-exponential Factors from Modeling (for single point solutions) 82

LIST OF FIGURES

Figure 2-1: Swelling Ratio vs Maximum Particle Heating Rate (Gale et al., 1995).	11
Figure 3-1: Flat Flame Burner and Collection Apparatus-(Hong, 2000).....	18
Figure 4-1: Collection Probe Height vs. HTVL plotted for various O ₂ conditions	
(Large Pitt8 coal at 10 atm.).....	22
Figure 4-2: Collection Probe Height vs. HTVL plotted for various O ₂ conditions	
(Large Pitt8 coal at 2.5 atm.).....	23
Figure 4-3: Char burnout curves for various pressures using Niksa-Hurt parameters	28
Figure 4-4: Particle temperature curves for various pressures using Niksa-Hurt parameters	28
Figure 4-5: Reaction order vs. particle temperature for two kinetic parameter sets.....	30
Figure 4-6: Char burnout curves for various pressures using Hurt-Calo parameters in	
the CCK-Oxy code	31
Figure 4-7: Particle Temperature curves for various pressures using Hurt-Calo parameters.....	31
Figure 4-8: Two χ factor curves vs. time during char particle burnout	35
Figure 5-1: 2.5 atm single point solution parity plot	43
Figure 5-2: 2.5 atm all O ₂ conditions solution parity plot	44
Figure 5-3: 6 atm single point solution parity plot	45
Figure 5-4: 6 atm all O ₂ conditions solution parity plot	45
Figure 5-5: 10 atm single point solution parity plot	46
Figure 5-6: 10 atm all O ₂ conditions solution parity plot	47
Figure 5-7: Parity plot generated using all available data.....	48
Figure 5-8: Parity plot generated using all available data from each pressure group.....	48
Figure 5-9: Absolute Error Statistical Comparison-All Modeling Methods	51
Figure 5-10: Char burnout vs. total pressure and partial pressure using the CCK code	
with the Hurt-Calo model.	56
Figure 5-11: Char burnout vs. total pressure and partial pressure using the CCK code	
with the Niksa-Hurt model.....	57
Figure 5-12: Comparison of char burnout at 5% O ₂ for various pressures and	
2 kinetic models	57
Figure 5-13: Burnout curves for various pressure- O ₂ combinations using the	
Niksa-Hurt model.....	58
Figure 5-14: Burnout curves for various pressure- O ₂ combinations using the	
Hurt-Calo model.	59
Figure 5-15: Char burnout bar charts at various pressures and fixed 5 mole % O ₂	
for two separate kinetic approaches.....	60
Figure 5-16: CO ₂ effects on char burnout at various pressures	61
Figure 5-17: Gas Temperature effects on char burnout at various pressures	62
Figure 5-18: Particle diameter effects on char burnout at various pressures	63
Figure 5-19: A ₃₀ effects on char burnout at various pressures.....	64
Figure B-1: Generated Black Thunder Coal Mass Conversion Data Prior to Lab Corrections....	76
Figure B-2: Generated Black Thunder Coal Mass Conversion Data after Lab Corrections	77
Figure C-1: Absolute Error Statistical Comparion using all Hurt-Calo modeling	80

Figure C-2: Absolute Error Statistical Comparison for 3 Kinetic Methods from A ₃₀	
values found using Each Pressure Group	80
Figure C-3: Actual Error Statistical Comparison-All Modeling Methods.....	81
Figure C-4: Actual Error Statistical Comparison using all Hurt-Calo modeling	81
Figure C-5: Actual Error Statistical Comparison for 3 Kinetic Methods from A ₃₀	
values found using Each Pressure Group	82

NOMENCLATURE

Parameters	Description	Units
A_1	Pre-exponential factor for the 1st surface reaction for Langmuir-Hinshelwood kinetics	$\frac{1}{s} * \left(\frac{cm^3}{mol}\right)$
A_2	Pre-exponential factor for the 2nd surface reaction for Langmuir-Hinshelwood kinetics	$\frac{1}{s} * \left(\frac{cm^3}{mol}\right)^n$
A_3	Pre-exponential factor for the 3rd surface reaction for Langmuir-Hinshelwood kinetics	$\left(\frac{1}{s}\right)$
A_{30}	Initial A_3 prior to the char oxidation occurring	$\left(\frac{1}{s}\right)$
A_n	Pre-exponential factor for the n^{th} -order reaction	$\left(\frac{gm}{s * cm^2 * atm^n}\right)$
E_{A1}	Activation energy for the 1st surface reaction for Langmuir-Hinshelwood kinetics	$\left(\frac{cal}{mol}\right)$
E_{A2}	Activation energy for the 2nd surface reaction for Langmuir-Hinshelwood kinetics	$\left(\frac{cal}{mol}\right)$
E_{A3}	Activation energy for the 3rd surface reaction for Langmuir-Hinshelwood kinetics	$\left(\frac{cal}{mol}\right)$
E_{An}	Activation energy for the n^{th} -order reaction	$\left(\frac{cal}{mol}\right)$
C	Mean concentration of O_2 inside the particle (assumed to be half of the surface concentration in Equation 10.)	$\left(\frac{mol}{cm^3}\right)$
C_s	Surface concentration of O_2	$\left(\frac{mol}{cm^3}\right)$
d	Char particle diameter	(cm)
d_o	Initial char particle diameter	(cm)
D_{O_2}	Diffusivity of O_2	$\left(\frac{cm^2}{s}\right)$
k''_m	Molar mass transfer coefficient	$\left(\frac{mol}{s * cm^2 * atm}\right)$
$k_{m,T_{max}}''$	Molar flux coefficient at the maximum particle temperature that occurs at the maximum burn rate	$\left(\frac{mol}{s * cm^2 * atm}\right)$
K_1	Rate constant for the 1st surface reaction for Langmuir-Hinshelwood kinetics	$\frac{1}{s} * \left(\frac{cm^3}{mol}\right)$
K_2	Rate constant for the 2nd surface reaction for Langmuir-Hinshelwood kinetics	$\frac{1}{s} * \left(\frac{cm^3}{mol}\right)^n$
K_3	Rate constant for the 3rd surface reaction for Langmuir-Hinshelwood kinetics	$\left(\frac{1}{s}\right)$

Parameters	Description	Units
m_p	Mass of the char particle	(gm)
$m_{p,0}$	Initial mass of the char particle	(gm)
n	Reaction order	(<i>unitless</i>)
n_{eff}	Effective reaction order used in calculating the Thiele Modulus	(<i>unitless</i>)
n_{O_2}''	Molar flux of O ₂ to the char particle	$\left(\frac{mol}{s * cm^2}\right)$
$n_{O_2,max}''$	Maximum molar flux of O ₂ to the char particle	$\left(\frac{mol}{s * cm^2}\right)$
P_T	Total system pressure	(atm)
$P_{O_2,\infty}$	Partial pressure of O ₂ in the bulk phase	(atm)
$P_{O_2,s}$	Partial pressure of O ₂ at the particle surface	(atm)
Q_n	Char oxidation rate for the n th -order reaction	$\left(\frac{gm}{s * cm^2}\right)$
Q	Char oxidation rate (general)	$\left(\frac{gm}{s * cm^2}\right)$
Q_{max}	Maximum char oxidation rate	$\left(\frac{gm}{s * cm^2}\right)$
R_{gas}	Universal gas constant	$\left(\frac{cal}{mol * K}\right)$
R_s	Intrinsic rate of combustion	$\left(\frac{1}{s}\right)$
<i>stoich</i>	The stoichiometric coefficient relating moles of O ₂ consumed to grams of carbon consumed.	$\left(\frac{mol_{O_2 \text{ consumed}}}{gm_{carbon}}\right)$
Sh	Sherwood number $\left(\frac{k_m'' d_p}{D_{O_2}}\right)$, assumed to be 2 in this work	(<i>unitless</i>)
T_g	Gas temperature	(K)
T_p	Particle temperature	(K)
α	The mode of burning parameter	(<i>unitless</i>)
χ	The Kai factor	(<i>unitless</i>)
η	The effectiveness factor for combustion	(<i>unitless</i>)
ρ	Char particle density	$\left(\frac{gm}{cm^3}\right)$
ρ_0	Initial char particle density	$\left(\frac{gm}{cm^3}\right)$
ϕ	The Thiele Modulus	(<i>unitless</i>)
y_{O_2}	Mole fraction of O ₂	$\left(\frac{mol O_2}{mol \text{ mixture}}\right)$

1. Introduction

Coal plays an important part in electricity production in America and will into the foreseeable future. While making up more than 20% (EIA, 2021) of the United States electricity portfolio, coal is nowhere near being replaced as a major energy source, and large reserves are available that would last centuries at our current usages. However, carbon emissions are becoming an ever-increasing concern to which coal is a large contributor.

While coal is not a “green” energy, there is a possibility to eliminate carbon emissions into the atmosphere through carbon capture. Cryogenic carbon capture (Baxter et al., 2009) is one method of doing so. However, oxy-coal combustion (Shaddix and Molina, 2009) is another that provides promising results, where the O_2 from air is separated and fed with coal to the boiler, usually with flue gas recycle to avoid excessively high temperatures. Oxy-coal boilers have near pure CO_2 outlet streams after H_2O separation, which makes for relatively easy carbon capture without much post-combustion treatment. There are currently around 240 coal boilers in operation in the United States and thousands worldwide which could potentially be retrofitted to become oxy-coal boilers as well as new ones that could be designed. The problem is that burning coal in an O_2 - CO_2 environment drastically changes the way that char oxidation occurs. To be able to retrofit existing boilers and create new ones, accurate models need to be developed that describe combustion in this type of environment.

This project underwent a shift midway through to include pressure research into the oxyfuel combustion due to a change in the goals of the funding agency. Accurate models also need to be developed to include pressure and seek to have a fundamental understanding of the physics involved in char combustion to be applicable to a wide range of coals and pressures.

Coal combustion at high pressure yields various benefits such as increased burn rate and potential environmental benefits as well. Increased burn rate can lead to increased coal throughput (Harris and Patterson, 1995) or even the design of smaller less expensive reactors. It has been shown that combustion at higher pressures can result in a reduction of NO_x emissions (Lasek et al., 2013). Improving the understanding of char oxidation at high pressure is key to the adopting of this technology and unlocking all of its potential.

This work is broken up into seven chapters. Chapter 2 contains a literature review that covers the basics of coal, coal conversion, pressure effects and other general principles. Chapter 3 lays out the objective and tasks specific to this thesis. Chapter 4 describes the high-pressure modeling approach taken with information about the data set used, a brief description of the char burnout code, and certain limitations and assumptions taken for this work. Chapter 5 presents the results and discussion for this work comparing various models and sensitivity analysis. Chapters 6 and 7 give the conclusions and recommendations.

2. Literature Review

2.1 Coal

Coal is comprised of fossilized organic material. It is made up of mostly carbon and hydrogen with some other elements such as oxygen, nitrogen, sulfur, and more trace elements. Coal is different from other common hydrocarbons such as propane or butane in that it is not a specific molecule but rather a large network of aromatic clusters and side chains. Coal is often characterized by elemental content or rank, and is subcategorized into 4 groups: lignite, subbituminous, bituminous, and anthracite (Hendrickson, 1975). Coal combustion characteristics depend highly on the parent coal rank (Smoot and Smith, 1985).

2.2 Coal Conversion

Regardless of the coal type, the overall processes within coal combustion remain similar. As heating occurs, particles follow a path of dehydration, devolatilization, and finally char oxidation. Dehydration (i.e., moisture evaporation) commences at lower temperatures. As the coal particle continues to heat up, pyrolysis occurs and light gases are released along with some of the heavier tars. Depending on the heating rate and pressure, the particle will swell to different degrees due to the increase in internal pressure from the releasing volatiles which changes the original particle size and properties. The remaining char is consumed through oxidation and gasification via many different reactions. As the char particle reacts, it becomes less reactive

over the course of the burn. This process of losing reactivity is referred to as annealing. As the oxidation and gasification go to completion, there is an ash portion that will not combust comprised of oxidized minerals.

2.3 Coal Conversion Modeling History

Over recent decades many models have been developed and improved to attempt to replicate the physics of coal combustion. The evolutionary process of model development has been a balance between including as many descriptions of physical reaction processes as possible to accurately model coal combustion and keeping the model simple such that the simulation can be efficiently run on a supercomputer. One of the most recent fundamental models is the Carbon Burnout Kinetics model (CBK) which was developed by Hurt et al. (1998). This work along with many of the subsequent works are summarized in Table 2-1.

The development of coal combustion modeling is an ongoing effort that sees improvement as reaction and mass transfer processes are discovered and modeled. Haugen and Mitchell recently summarized much of the work around the various numerical approaches for the conversion of char (Haugen et al., 2022). Research on coal combustion modeling is ongoing, specifically in oxy-coal conditions as well as with high pressure conditions.

Table 2-1 Recent Coal Conversion Modeling History

Model	Features	Author (Date)
CBK (Carbon Burnout Kinetics)	<ul style="list-style-type: none"> ▪ Particle reactivity variation model ▪ Single-film char oxidation model ▪ Thermal deactivation model ▪ Physical property model 	Hurt et al. (1998)
HP-CBK (High Pressure)	<ul style="list-style-type: none"> ▪ Intrinsic rate equation rather than n^{th}-order kinetics ▪ Analytical solution of effectiveness factor for Langmuir rate equation with correction factor ▪ Pore structure model included for calculation of effective diffusivity (Knudsen and molecular) 	Hong (2000)
CBK/E (Extended)	<ul style="list-style-type: none"> ▪ Improved oxidation kinetics ▪ 3-step semi-global mechanism ▪ Simple for computational models ▪ 3 Arrhenius type kinetic expressions 	Niksa et al. (2003)
CBK/G (Gasification)	<ul style="list-style-type: none"> ▪ Gasification rate laws ▪ Associated effectiveness factors ▪ A pore evolution description 	Liu and Niksa (2004)
CCK (Carbon Conversion Kinetics)	<ul style="list-style-type: none"> ▪ 8-step mechanism for gasification and oxidation ▪ Transport equations, kinetics, and effectiveness factors for the above reactions ▪ Film diffusion, pore diffusion, ash encapsulation, and annealing 	Shurtz and Fletcher (2013)
CCK/Oxy (Oxy-Coal Conditions)	<ul style="list-style-type: none"> ▪ Several sub-models adjusted with more realistic physics/extended to oxy-coal conditions: ▪ Annealing model, swelling model, mode of burning parameter, kinetic model addition of the chemical percolation devolatilization (CPD) model. 	Holland and Fletcher (2017)

2.4 Oxy-Coal Combustion Modeling

Oxy-coal combustion consists of reacting pulverized coal with O₂/CO₂ mixtures as opposed to a largely O₂/N₂ mixture. The main goal is to capture CO₂ more easily. Elevated concentrations of O₂ may be used to achieve higher temperatures for higher thermodynamic power production efficiencies. Current materials, however, are not adequate to contain combustion temperatures in high-temperature oxy-fuel technology. Therefore, the current primary method of adapting to this is to recycle CO₂ back into the combustion environment to

effectively dilute the heat. The O_2/CO_2 environment changes the manner in which the coal reacts and must be modeled appropriately. Hecht et al. (2012) showed that replacing the N_2 in the reactive environment with recycled CO_2 changes transport properties, radiation transport, and bulk gas heat capacity. Char gasification reactions become increasingly important as well.

Several fundamental studies of oxy-char combustion have been conducted. For example, Shaddix and Molina (2009) performed 2 color-pyrometry experiments to measure particle temperatures of reacting char particles in an $O_2/CO_2/H_2O$ environment. They were able to show that CO_2 retards single-particle coal ignition and has a small effect on the duration of volatile combustion. Increased O_2 concentration accelerates particle ignition. Their measurements were performed with an average particle size of 100 microns. This is about twice the size of average particles in industrial burners. It was necessary to use larger particles in this study because optical pyrometry experiments are easier with large particles since the small particles burn out quickly and drop to temperatures below the optical measurement threshold.

Geier et al. (2012) also performed oxy-coal combustion experiments and extended a single film n^{th} -order Arrhenius char oxidation model to include CO_2 and H_2O gasification reactions. They produced parameters that fit the two-color pyrometry data well, however, the parameters were physically meaningless. The best fits for activation energy or pre-exponential factors were either zero or negative, which seemed nonsensical. They suggested several possible reasons for the strange parameter values, such as the lack of CO conversion in the particle boundary layer in their approach.

Most recently, Holland and Fletcher (2017) adapted the CCK model to oxy-coal conditions and compared the generated results with the sets of data from Shaddix and Molina (2009) which matched very well. A new annealing sub-model was created along with

improvements within devolatilization, swelling, and mode of burning parameter models (Holland et al., 2017).

While it is apparent that much progress has been made in modeling oxy-coal combustion, it is also evident that most of the work performed in this area is derived from a limited set of optical experiments. If the models generated could be adapted for data sets that measured mass conversion, much more confidence could be placed in model predictions.

2.5 High Pressure Char Oxidation Data Sets

Char oxidation has been extensively studied over the past few decades and the kinetics for atmospheric systems are fairly well understood. However, high pressure char combustion kinetics are much more of an unknown. Table 2-2 below summarizes much of the limited set of relatively recent work involving high-pressure char oxidation.

Table 2-2: High Pressure Combustion Data Sets

Investigator(s)	Fuel	Diameter (μm)	T_g (K)	P_{total} (atm)	Y_{O2} (%)
Monson et al. (1995)	Chars	40-70	1000-1500	1-15	5-21
Mathias (1996)	Coals and chars	Mostly 8000	900-1200	0.86-5	4-21
Ranish and Walker (1993)	Graphite Flakes	1-200	733-842	1-64	100
Banin et al. (1997)	Chars	5	1200-1800	7-9	0-100
Croiset et al. (1996)	Chars	90-106	850-1200	2-10	1.5-10
MacNeil and Basu (1998)	Chars	417-2000	973-1123	1-7	10-21
Zeng (2005)	Chars	63-125	800-1800	1-15	0-19.2

Table 2-2: High Pressure Combustion Data Sets (Continued)

Investigator(s)	Fuel	Diameter (μm)	T _g (K)	P _{total} (atm)	Y _{O₂} (%)
Ying et al. (2016)	Chars	<74	1173	1-20	21-50
Pang et al. (2021)	Chars	2,800-3,350	1173	1-5	10-30

Char oxidation modeling has shown different kinetic forms. One common method is nth-order global kinetics. Equation 1 below shows a rate expression using an nth-order expression.

$$Q_n = A_n * e^{-\left(\frac{E_{a,n}}{R_{gas} * T_p}\right)} * P_{O_{2,s}}^n \quad (\text{Eq 1})$$

Nth order modeling is generally able to fit data at specific conditions; however, it is frequent that this type is unable to have parameters that work over a range of conditions. Langmuir-Hinshelwood kinetics seek to better describe the reaction. Equation 2 shows an expression for a L-H intrinsic rate calculation. Further equations relate this intrinsic rate expression to a char oxidation rate in section 4.4.2.

$$R_s = \frac{K_2 * C_s^{n+1} + K_3 * C_s}{C_s + \frac{K_3}{K_1} * \frac{1}{2}} \quad (\text{Eq 2})$$

Langmuir-Hinshelwood kinetics considers separate molecules that absorb to a surface before reacting. Attempts at modeling high pressure have been repeatedly more successful using Langmuir mechanisms. Monson et al. (1995) showed that “atmospheric pressure global model parameters cannot be accurately extrapolated to elevated pressures.” Their work performed in a

drop tube reactor demonstrated that n^{th} -order kinetic extrapolations result in much higher temperatures and reaction rates than in normal processes and are therefore insufficient.

Ranish and Walker (1993) used the Langmuir model to explain reaction order and apparent activation energy changes with temperature and pressure. Croiset et al. (1996) found the Langmuir isotherm was well suited at elevated pressure; although, the char was prepared at very low heating rates (10 K/min) and at atmospheric pressure. However, they showed a decrease in pre-exponential factor with increasing pressure which is not theoretically supported. Essenhigh and Mescher (1996) developed a method using a “second effectiveness factor” and were able to accurately model Monson and Germane’s data. They also suggested that pressure affects reaction penetration which is why reactions are pressure dependent.

Hong et al. (2000) and Hecker et al. (2003) both studied high-pressure effects on char oxidation with char generated at high heating rates (10^5 K/s). Hong explored how the gas composition ($\text{H}_2\text{O}/\text{O}_2$) surrounding the particle affects char properties due to the annealing process. He adapted the original CBK model to be better suited for high pressure conditions by including Langmuir kinetics as well as an analytical effectiveness factor, a pore structure model, and Nusselt and Sherwood correlations. His model was successful at matching char oxidation data over a large range of conditions. Hecker was successful at using n^{th} -order kinetics to fit high-pressure TGA data. He also showed that the kinetic parameters determined were independent of pressure. However, the chars that Hong and Hecker studied were generated at atmospheric pressure and would therefore not include pressure effects on char preparation. Zhang (2019) did the opposite of Hecker by forming the char at pressure and then performed TGA experiments at atmospheric pressure. He found that the rate of combustion was dependent on the formation pressure.

Zeng (Zeng, 2005; Zeng et al., 2005) performed char oxidation experiments in a pressurized flat-flame burner system, and then performed thermogravimetric (TGA) char reactivity measurements at the pressures at which the char particles were formed. Zeng's results differed from what Hecker found indicating that the formation pressure plays a part in the reactivity of the resulting char. Zeng also performed char oxidation experiments with the high-pressure flat-flame burner and tried to fit the char burnout data with the CBK model but had to use a different activation energy for each pressure.

2.6 Swelling and Annealing

A key factor in modeling char oxidation is knowing that the formation of char is path dependent. In other words, char reactivity depends on the conditions in which the char was formed. Heating rate and pressure affect swelling characteristics during coal pyrolysis and consequently the annealing as well. While many principles have been learned in the way of pressure testing, most of that work is done using TGA analyzers and some drop tube reactors. The TGA data sets are only semi-useful since they were performed at low temperatures and heating rates which do not mimic industrial conditions.

As seen in the figure below, the heating rate (which varies significantly across experimental apparatuses), significantly affects the swelling ratio and consequently the char reactivity. Therefore, it is much more useful to use chars formed as close as possible to industrial rates of 10^6 K/s. Figure 2-1 below (Zygourakis, 1993; Gale et al., 1995) shows some of the major trends that heating rate has on swelling.

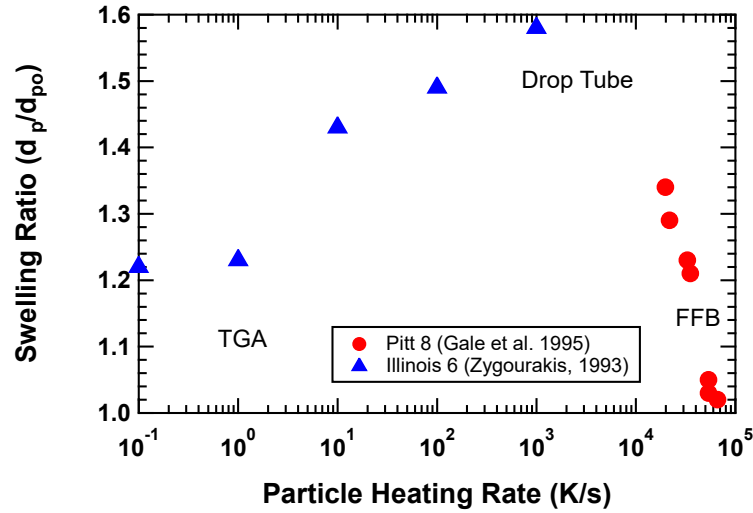


Figure 2-1: Swelling Ratio vs Maximum Particle Heating Rate (Gale et al., 1995).

Pressure also greatly affects swelling. These changes translate to the composition of the resulting char as well. As explained in a previous section, as the coal particle heats up light gases and tars release from the “coal matrix.” Changes in yields of tar and light gas at different pressures have been successfully modeled using vapor pressure principles. If surrounding pressure is increased during char formation, heavier tars are not as easily released, thus changing the composition, structure, and reactivity of the resulting char. The most recent CCK/Oxy code uses the Chemical Percolation Devolatilization model to help describe this trend (Fletcher et al., 1992).

Ma and Mitchell (2009) researched how the density and size of a char particle change as it reacts. The parameter to describe this relationship is known as the mode of burning parameter (α). Equation 3 uses the parameter to relate the change in density and mass of a char particle:

$$\frac{\rho}{\rho_o} = \left(\frac{m_p}{m_{p,o}} \right)^\alpha \quad (\text{Eq 3})$$

For a constant change in density α is 0. For a constant change in diameter α is 1. Further algebraic manipulation leads to another form (Equation 4) that relates the change in diameter to the change in mass.

$$\frac{d}{d_o} = \left(\frac{m_p}{m_{p,o}} \right)^{\frac{1-\alpha}{3}} \quad (\text{Eq 4})$$

Ma and Mitchell were able to show that this parameter could be related with an effectiveness factor which was determined by the Thiele modulus. Different equations exist depending on whether a reaction is diffusion limited, kinetic limited, or a combination of both. They also noted that the variations in char increases as pressure increases during coal combustion.

Zeng et al. (2005) used a high-pressure flat-flame burner (HPFFB) to create char at different pressures at higher heating rates of 10^5 K/s which was a significant improvement. Shurtz et al. (2011) furthered this work and built a new swelling model that takes heating rate, pressure, and coal rank as inputs, improving upon a model reported by Liu and Niksa (2004). Yang et al. (2014) developed a detailed swelling model including the effect of heating rate and pressure.

2.7 Char Formed at Pressure

The pathway by which char is formed affects the structure. The formation pathway includes pressure, and swelling is not the only feature affected by pressure. There have been various studies over the past two decades that describe some of these effects. One study showed that char formed at high pressure compared to atmospheric conditions showed large morphology

and internal structural differences (Yu et al., 2004). Higher pressure favors more foam type and less cenospheric or solid. The char is more swollen with higher porosity. This was true across multiple heating rates demonstrated in a drop tube and entrained flow burners. Another study showed that pressure bubble coalescence and porosity increased with increasing pressure (Hao et al., 2016). The formation of mesopores are also more favorable at high pressure (Zhang et al., 2019).

Not only is the physical shape of the char changed by char formation conditions but also the chemical structure of the char that is left behind after pyrolysis. Increasing pressure for char formation enhances the decomposition of functional groups resulting in a higher ordering of the carbon structure (Tahmasebi et al., 2018). Other studies further show that the graphitization degree (turning smaller aromatics into larger ones) increases with pressure, and that the fraction of carbon-carbon bonds (both double and single) increases while the fraction of carbon-hydrogen bonds decreases (Lei et al., 2018) and (Zhang et al., 2019).

Another interesting trend is that as pressure increases the environment in which the char is formed also affects the char. The role of the atmosphere becomes evident beyond 5 atm. There is an increase in hydroxyl, secondary hydroxyl, olefinic carbon-carbon bonds, and aromatic carbon structure for char prepared in a CO₂ environment compared to when it is made in an argon atmosphere (Bai et al., 2013).

Consequently, while studies that explore the effects of pressure on char oxidation for char generated in an atmospheric environment are informative from a kinetics perspective (Hecker et al., 2003), a more complete understanding of combustion at pressure requires studying chars generated at the same pressure as the subsequent char conversion study.

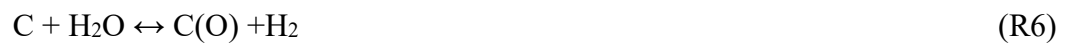
2.8 Surface Kinetics

Surface kinetic schemes describe what reactions occur that govern the overall carbon burnout process. Shurtz and Fletcher (2013) created two different Char Conversion Kinetic versions: CCK^N which utilized nth-order kinetics and CCK which utilized a semi-global Langmuir-Hinshelwood kinetic mechanism that combines the 5-step gasification and 3-step oxidation reactions. The 8 reactions for the CCK model are shown below, where C(O) represents an oxygen atom adsorbed to a carbon site.

Oxidation:



Gasification:



2.9 Summary

Holland and Fletcher (2017) created the most recent coal combustion modeling code (CCK/Oxy) that treats most of the discussed principles very well including swelling, annealing, and kinetics for the 8-step combined gasification-oxidation reactions shown above. Their work has proven adequate to accurately model char oxidation in oxy-fuel conditions with the available data sets. However, prior to this work, the CCK/Oxy code had not been compared to any high-pressure data sets.

3. Objective and Tasks

The main objective of this project is to model the high-pressure high heating rate entrained flow data set created by Dong Zeng (referred to as DZ) using the CCK model. This will include solving for pre-exponential factor for the rate controlling step in the Langmuir-Hinshelwood kinetic model at various pressure conditions. The predicted results vs. the experimental data is compared for two kinetic input parameter variations (Hurt and Calo, 2001) and (Niksa et al., 2003) which are referred to as HC and NH respectively. These results are also compared to the modeling results of the CBK code (Zeng, 2005). Further, a sensitivity analysis was performed. Specific tasks are listed below.

- Task 1: Analyze the DZ high-pressure high heating rate data set by using the CBK model to determine what the residence time and collection heights were in the original experiments.
- Task 2: Model the DZ data set using the CCK-Oxy Code. Produce prediction burnout curves for two kinetic input parameter variations (NH and HC) and compare the results alongside the DZ results obtained with the CBK model.
- Task 3: Perform a sensitivity analysis on various parameters within the CCK code using the pre-exponential factors obtained from fitting the DZ data. The parameters that will be varied are pressure, temperature, gas composition (O_2 and the remaining environment), heating rate and diameter.

Task 4: Obtain additional oxy-fuel char oxidation data sets using a flat-flame burner at atmospheric pressure.

Task 1. Complete the DZ Data Set by Determining Residence Time

The DZ high-pressure high-heating rate entrained-flow data as recorded in his dissertation is not a complete data set since it is lacking sampling heights (and corresponding residence times). However, since Zeng showed some modeling results, the original reported results were used here to effectively solve for what the heights must have been. The HTVL (High Temperature Volatile Loss) used in the modeling was also not specified. After communicating with Dong Zeng, the assumption was made that for a given coal type, diameter, and pressure condition that the same collection probe height was used for the different O₂ conditions. The collection heights and consequently the residence times were then graphically determined with the help of the published velocity profiles.

Task 2. Model the DZ High Pressure High Heating Rate Data Set

The DZ data were modeled using the CCK code. Input parameters such as system pressure, O₂ partial pressure, velocity and temperature profiles, diameter and others were extracted from the DZ data set and input into the CCK code. One of the outputs, char burnout fraction, was compared to the actual char burnout data and the pre-exponential factor was adjusted to solve for the best fit. This was done for individual pressure conditions as well as for

the whole data series. Results were obtained for two separate kinetic input values (NH and HC). Further, the two CCK methods along with the DZ results using the CBK were compared.

Task 3. Perform a Sensitivity Analysis with the CCK Code

Using the CCK model with the pre-exponential factors solved from the DZ data, environmental parameters were then adjusted and charts were generated that show burnout curves and particle temperature profiles. The environmental parameters that were adjusted are as follows: total pressure, O₂ partial pressure, remaining gas composition, gas temperature, particle diameter, particle heating rate, and kinetic parameters. A chart is generated for each showing the relative effect of the changes for the various pressures.

Task 4. Atmospheric FFB Experiments

Experiments were conducted with a flat flame burner at oxy-fuel conditions, high heating rates (10^5 K/s), atmospheric pressure, and 43-53 μm particles. Black Thunder (Wyoming subbituminous), Sufco (Utah bituminous), and Illinois #6 (bituminous) were the 3 test coals for these experiments. Data were generated for a minimum of 2 temperatures (adiabatic flame temperatures of 1450 K, 1600 K, and sometimes 1750 K), 2 different gas compositions, and 4 different collection heights which adjusts the residence time. The heights for each coal varied since their reactivities varied as well. The repeatability of the experiments was improved after making modifications to the lab and flat flame burner set up. Due to the shift in the project goals, the results for this section were moved to appendix B.

Figure 3-1 shows a diagram of the flat-flame burner system. Fuels and oxidizers flow into the flat-flame burner to mix at the surface. A flat flame is generated by many small (approx. 1 mm) flamelets which creates the off-gas composition for the desired reacting environment. Pulverized coal is fed through a feed tube and into the reaction environment for a specified height at a fixed velocity from which residence time were calculated.

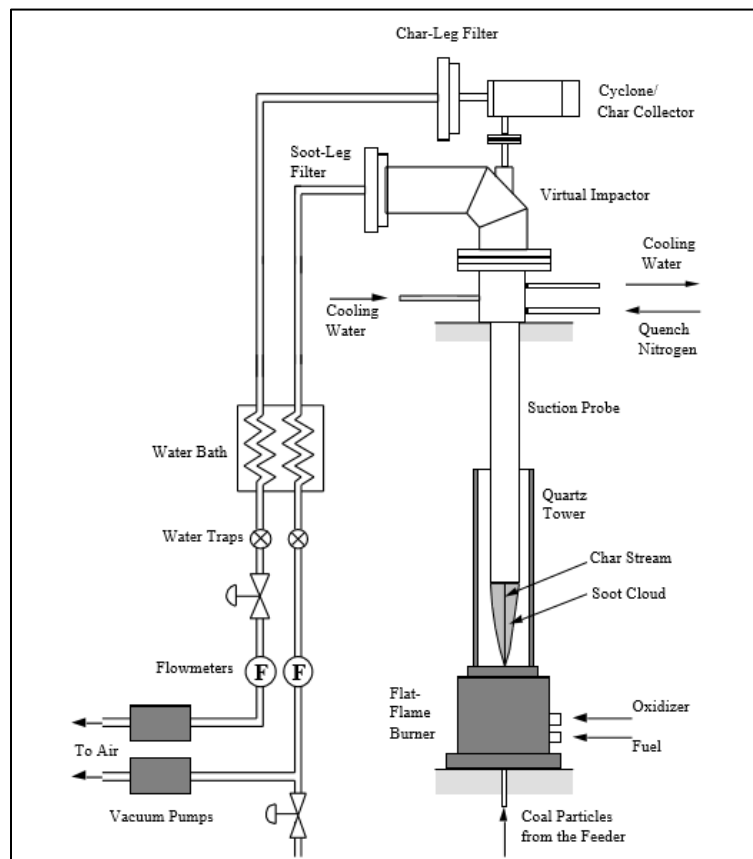


Figure 3-1: Flat Flame Burner and Collection Apparatus-(Hong, 2000)

The collection probe blows in cool nitrogen gas that extinguishes the burning coal particles. The particles are then pulled through the apparatus via a vacuum system, and a cyclone char trap

collects the particles which can be analyzed for mass conversion. More detailed descriptions of this experiment are provided by Ma (1996) and Hong (2000).

4. High Pressure Modeling Approach

This section describes details and challenges encountered when modeling the data, including why the DZ data set was chosen and efforts taken to make it a complete data set. The CCK code is described in general, with more detail on some of the subroutines and the effects of pressure in the code. The importance of the kinetic parameters chosen and the early setback that occurred due to having incorrect ratios in the code are also described. An explanation of the setbacks experienced in the CCK code with regards to the χ factor and the resolution to the diffusion restriction scenario are given.

An assumption was made in this modeling approach that the gasification reactions were negligible in relation to the oxidation reactions at these conditions.

4.1 Uniqueness of the DZ Data Set

Of the many data sets in the literature describing pressurized combustion, the DZ data set is unique in that it is the only one with the following: high-pressure, high-temperature, high-heating rate, entrained flow, char oxidation data using mass collection. The first four environment conditions are important because they most resemble the environment of an industrial scale coal combustion reactor. This is important for the overall modeling of individual coal particles inside of a reactor. The last item (mass collection) is important because mass loss data constitute an accurate method to measure the burning rate. Pyrometry measurements can be

skewed by missing small particles since their light may not be captured by the reading as mentioned in the literature review.

4.1.1 Incomplete Data Set

It is important to note that searching through the inputs of the code through Zeng's dissertation that the height of the collection probe for each experiment was not reported. The height of the collection probe for the various experiments could have been used to determine residence time. The sampling height or residence time was not found in any lab notebooks, old computer files at BYU or in the possession of Dong Zeng. However, plots of CBK model curve fits to the burnout data as a function of particle residence time were reported in Zeng's dissertation (Zeng, 2005). For this reason the residence time and subsequently the collection probe heights were solved for by running the original CBK code to match the final calculated burnouts from the data set produced by Zeng (2005).

4.1.2 Solving for Residence Time

If all but one of the input parameters (excluding residence time) to the CBK code and output (char burnout) were known, then solving for the residence time would have been a very straightforward operation. That would have simply been to use the Fortran CBK code and all input parameters to find the time at which the output matched the experimental char burnout results.

However, the HTVL (high temperature volatile loss) results for each of the runs were not specified either, so an approach was developed to graphically determine the HTVL input and the

residence time simultaneously. For a given pressure condition the HTVL is the same, independent of the O₂ partial pressure.

Determining the heights followed the following process. For a given pressure condition and coal type, a guessed value of HTVL was selected, burnout curves were generated for each O₂ condition that showed coal burnout for each time step. Cross referencing the modeled coal burnout data from the DZ data set, linear interpolation yielded the residence time for that particular HTVL guess. Using the published velocity profiles generated by Zeng (2005) in Fluent for each condition, a height was calculated from the corresponding residence time. This was repeated for many HTVL guess values and the produced heights were plotted against the HTVL values. Figure 4-1 shows that for the large Pitt8 coal at 10 atm, the collection heights merge just below 0.48 inches and this is the assumed height for the further modeling.

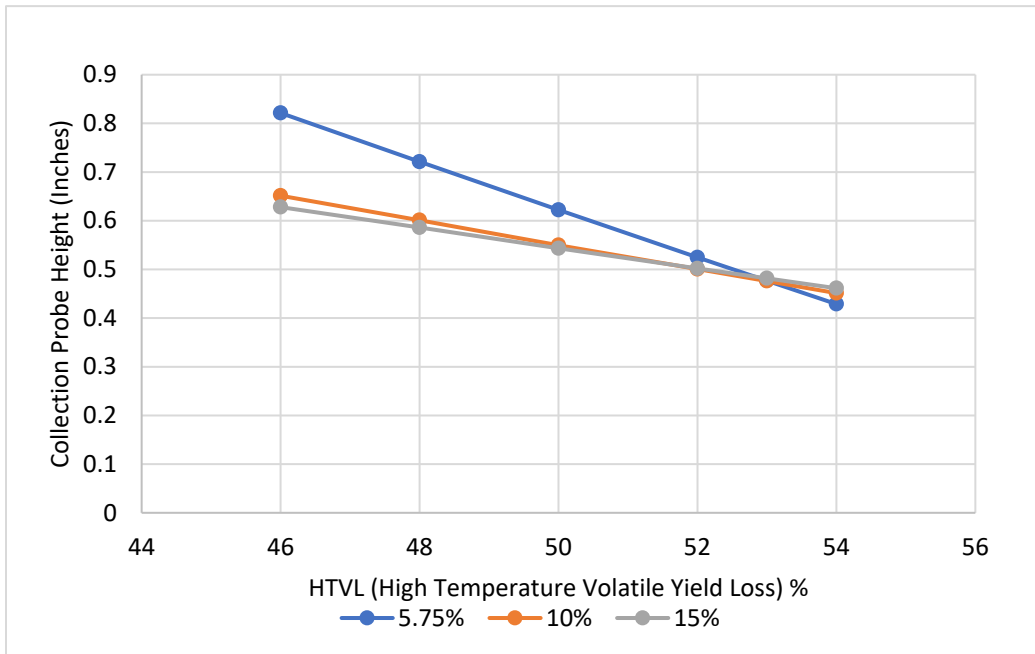


Figure 4-1: Collection Probe Height vs. HTVL plotted for various O₂ conditions (Large Pitt8 coal at 10 atm.)

As a further check to this method there was one piece of information to validate these findings. In Zeng’s dissertation, there is a sample code that gives a value of 55.17 for the HTVL for large Pitt 8 at 2.5 atm. This value was used as one of the HTVL guesses and included in the plot in Figure 4-2 below. The black “X” denotes this position on the chart. While the 2.5 atm condition doesn’t show as clean of a merge as the 10 atm, it is a reassurance that the best agreement between the curves happens at the HTVL listed in the sample code for that condition.

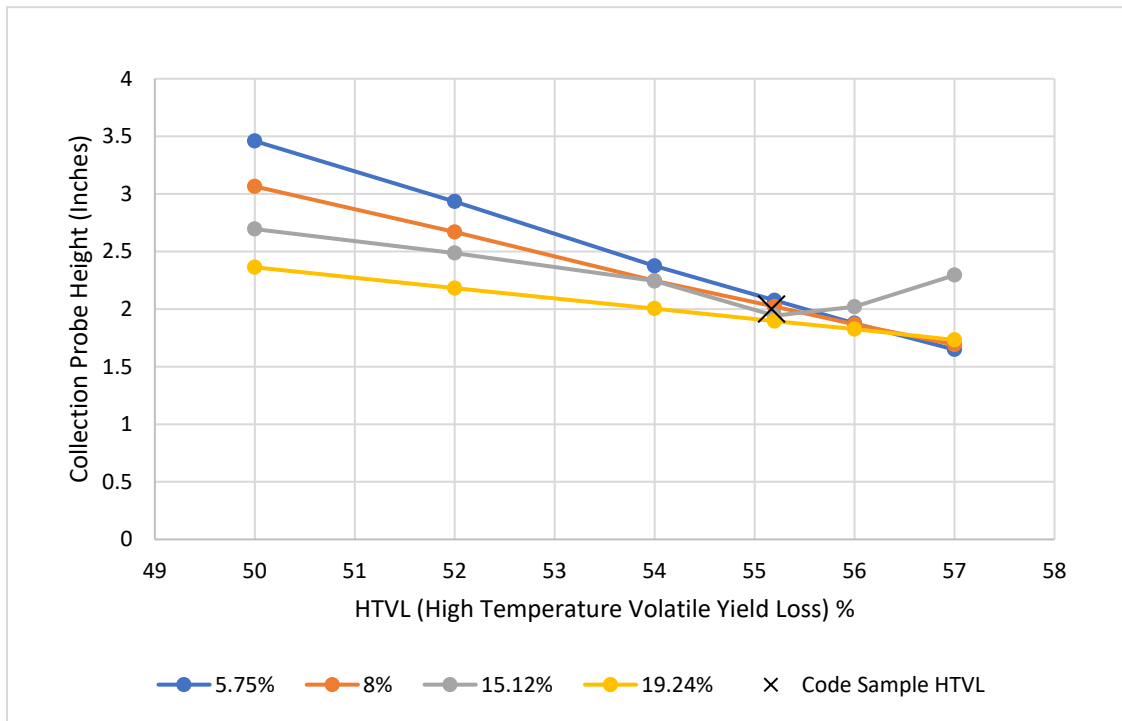


Figure 4-2: Collection Probe Height vs. HTVL plotted for various O₂ conditions (Large Pitt8 coal at 2.5 atm.)

Table 4-1 shows the results of the recreated residence times corresponding to the estimated probe locations by the method described. The same method was performed for the

other coal types from Dong Zeng's work (Pitt 8 small and Ill 6 for the short and long residence time) but the analysis didn't come out as clean.

Table 4-1: Recreated Residence Times for the Large Pitt 8 Coal Sampling Locations

Pressure Condition	Residence Time (ms)
2.5 atm	55.7
6 atm	76.4
10 atm	44.8

The inability to show the same trends for the other coal type and diameter may be due to the uncertainty in the modeled velocity profiles that were generated in Fluent by Zeng. The largest particles (Pitt 8 Large) may have had the most accurate flow modeling. Another explanation is that the heights for some of the conditions may not have been all the same. Smaller particles may have neared complete burnout for the higher O₂ atmospheres and so a shorter residence time may have been needed. Larger particles may have allowed for more flexibility to have all collection points at one height for a pressure condition. For these reasons the large Pitt 8 particle data were used for the analysis of sampling locations.

4.2 CCK Code

The most recent carbon burnout code (CCK/Oxy) was obtained from Holland in Matlab form. This is a single particle burnout model with various subroutines attempting to replicate the physics of burning a particle.

4.2.1 Subroutine Descriptions

The CCK/Oxy model is the most up-to-date model to describe char combustion, containing many improved sub-models, including: devolatilization, swelling, mode of burning parameter, diameter/density changes, annealing, pore diffusion, film diffusion, and CO/CO₂ formed at the particle surface. While shown to be successful for atmospheric oxy-coal conditions, CCK/Oxy had not been previously tested for high pressure (Holland (2017)).

4.2.2 Effects of Pressure in the CCK Code

This section describes where total pressure and O₂ partial pressure are referenced within the CCK/Oxy code. Total pressure and partial pressure of reactants are input parameters and will be addressed separately. Total pressure has various effects within the CCK-Oxy code. Pressure affects the chemical percolation devolatilization (CPD) model. From a physical standpoint, the pressure affects the overall mass release and the composition of the mass that remains. The tar yield and the H/C and O/C ratios change with pressure, for example. The swelling model is also affected by pressure. Particles that are formed at higher pressures tend to swell more (Zeng 2005) increasing the diameter. For a given partial pressure of O₂, increasing pressure will lower the mole fraction and all associated properties. Diffusion is also greatly affected by pressure. Equation 5 shows that the molar flux coefficient is proportional to the diffusivity of the reactant (O₂) and inversely proportional to the total pressure.

$$k''_m \propto D_{O_2} \propto \frac{1}{P_T} \quad (\text{Eq 5})$$

The sensitivity analysis in section 5.2.1 shows the combined effects of adjusting the total pressure while maintaining the partial pressure of O₂.

Adjusting the partial pressure of O₂ also plays many roles. Increasing the partial pressure has the inverse effect of increasing the overall pressure on mole fraction and all the dependent properties. The driving force behind diffusion is proportional to the difference between the bulk O₂ and surface partial pressures as shown in equation 6.

$$n_{O_2}'' = k''_m * (P_{O_2,\infty} - P_{O_2,s}) \quad (\text{Eq 6})$$

A major effect of increasing the partial pressure of O₂ is changing the reaction rate. The following set of equations yield the reaction rate “Q”. Changing the partial pressure of the equations will affect these equations anywhere that “C” or the concentration is listed.

$$K3 = A_3 * \exp\left(\frac{-E_{A3}}{R_{gas}*T_P}\right) \quad (\text{Eq 7})$$

$$K2 = A_3 * \frac{A_2}{A_3} * \exp\left(\frac{-E_{A2}}{R_{gas}*T_P}\right) \quad (\text{Eq 8})$$

$$\frac{K3}{K1} = \frac{A_3}{A_1} * \exp\left(\frac{E_{A1}-E_{A3}}{R_{gas}*T_P}\right) \quad (\text{Eq 9})$$

$$n_{eff} = \frac{(n+1)*K2*(C^n+K3)}{K3+K2*C^n} - \frac{1}{1+\frac{K3}{K1}*\frac{1}{2C}} \quad (\text{Eq 10})$$

$$R_s = \frac{K2*C_s^{n+1}+K3*C_s}{C_s+\frac{K3}{K1}*\frac{1}{2}} \quad (\text{Eq 11})$$

$$\phi = \frac{d}{6} \sqrt{\frac{n_{eff}+1}{2*d} * \frac{R_s}{C_s} * \frac{\rho}{stoich}} \quad (\text{Eq 12})$$

$$\eta = \begin{cases} \phi > 10 & \frac{1}{\phi} \\ 10 > \phi > 0.1 & \frac{1}{\phi} * \left(\frac{e^{3\phi} + e^{-3\phi}}{e^{3\phi} - e^{-3\phi}} - \frac{1}{3\phi} \right) \\ 0.1 > \phi & 1 \end{cases} \quad (\text{Eq 13})$$

$$Q = \frac{d}{6} * \eta * R_s * \rho \quad (\text{Eq 14})$$

All of the properties that will affect reaction rate subsequently affect temperature which also changes most of the subroutine calculations.

4.3 Kinetic Considerations

Kinetic parameters play an important part in the response to pressure. The original CCK-Oxy code was not adapted to handle pressure in this way. This was discovered early on while doing some sensitivity analysis. Original calculations with the CCK-Oxy code indicated that char burnout fraction and temperature profiles were independent of pressure. As shown in Figures 4-3 and 4-4, changing the pressure from 2.5 to 6 and 10 atm no perceptible change occurs. Note that these runs at the various pressures were performed at a constant mole fraction of O₂.

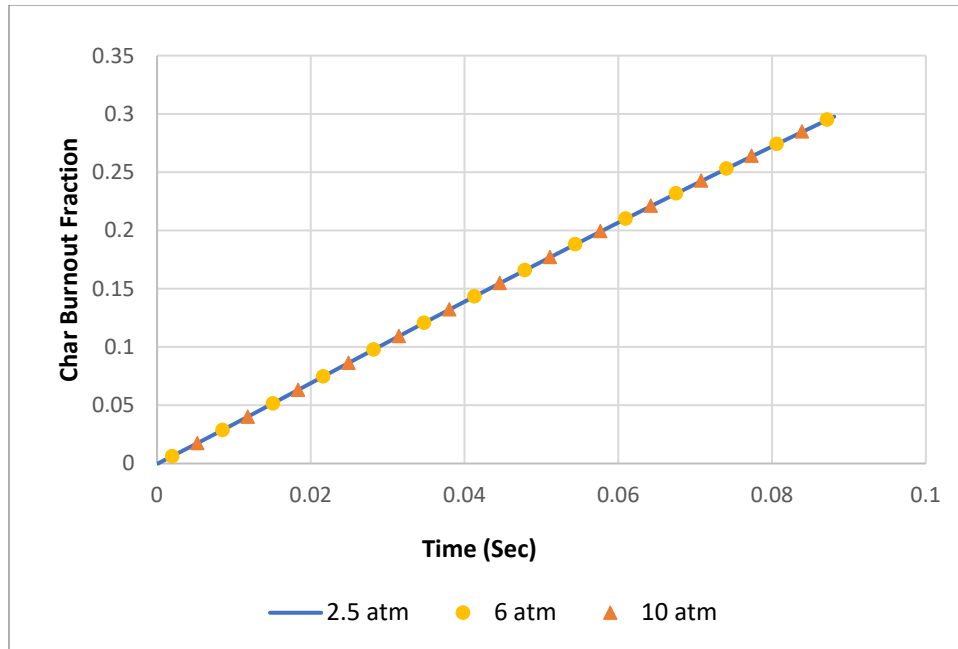


Figure 4-3: Char burnout curves for various pressures using Niksa-Hurt parameters using the initial version of the CCK-Oxy code

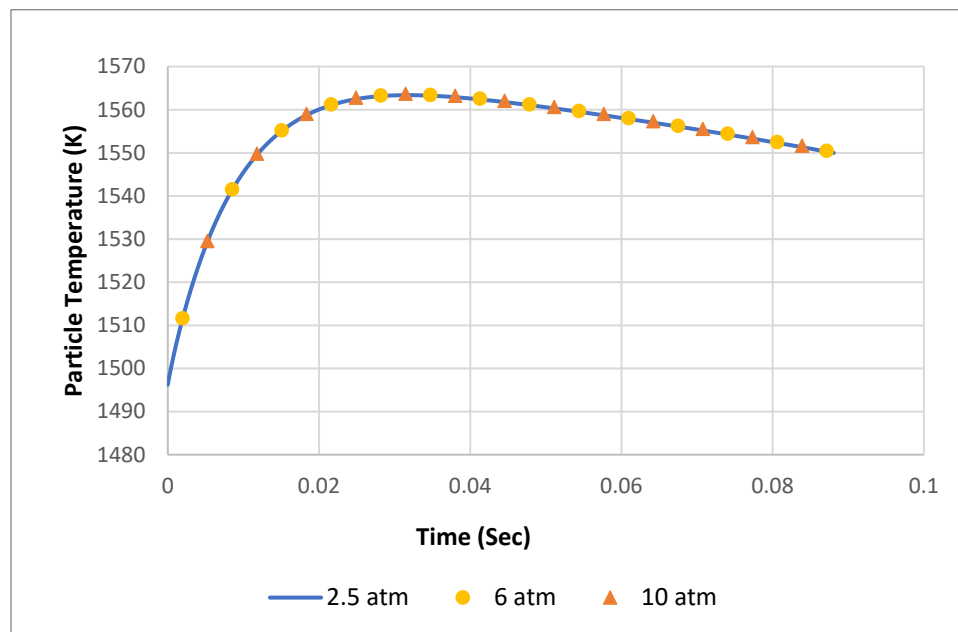


Figure 4-4: Particle temperature curves for various pressures using Niksa-Hurt parameters using the initial version of the CCK-Oxy code

Kinetic parameters were investigated due to the trends shown above. Hurt-Calo parameters presented an alternative. Table 4-2 shows the values used for each set.

Table 4-2: Kinetic Parameters: Niksa-Hurt and Hurt-Calo

Kinetic Parameter	Niksa-Hurt	Hurt-Calo	Units
$\frac{A_2}{A_3}$	5.0×10^4	5.7×10^{-4}	$\left(\frac{cm^3}{mol}\right)^N$
$\frac{A_3}{A_1}$	1.0×10^{-6}	3.0303×10^3	$\left(\frac{mol}{cm^3}\right)$
E_{A3}	3.198×10^4	4.302×10^4	$\left(\frac{cal}{mol}\right)$
E_{A2}	3.796×10^4	3.107×10^4	$\left(\frac{cal}{mol}\right)$
E_{A1}	5.975×10^3	5.633×10^3	$\left(\frac{cal}{mol}\right)$

The HC parameters were created with the intent to show a difference in reaction order across temperature regimes. Various data sources show that at low temperatures (less than 400 K), the reaction order is near 1. At mid-range temperatures (600 K to 1000 K) the reaction order is around 0. Finally, at higher temperatures (greater than 1400 K) reaction order increases up to a value near 1 again. Using HC parameters replicates this trend. This contrasts with what is seen by using the Niksa-Hurt parameters where the reaction order is near one for the entire temperature regime. Figure 4-5 models the reaction order for both kinetic sets and demonstrates

this trend. While NH parameters may have been useful to model a specific set of data, it does not appear to support yielding various reaction orders across various pressures.

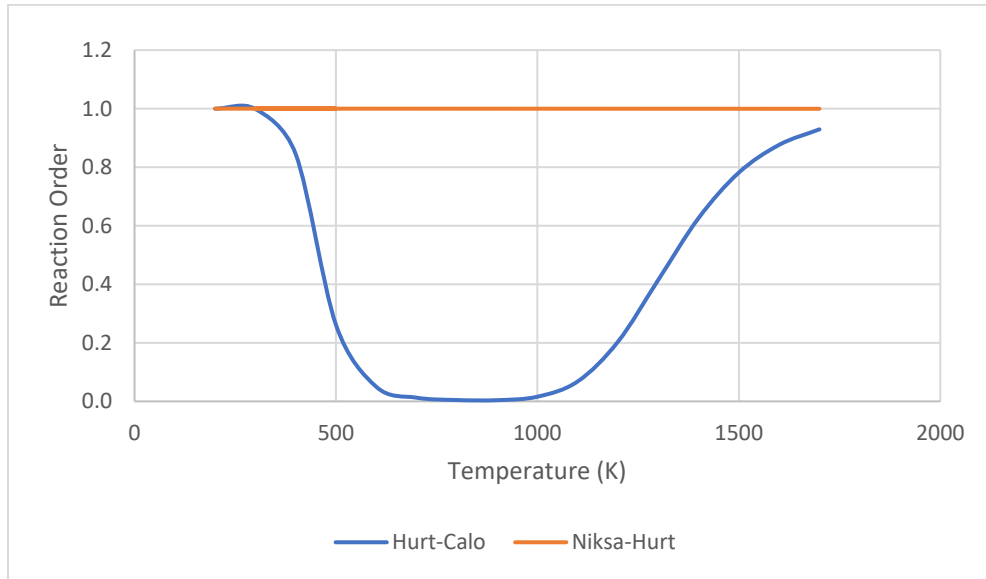


Figure 4-5: Reaction order vs. particle temperature for two kinetic parameter sets

When using the HC parameters in the CCK-Oxy code differences can be seen when varying the pressure. Figure 4-6 shows that increasing the pressure from 2.5 atm to 10 atm yields a higher burnout fraction using the HC parameters. This means that the set of kinetic parameters chosen affects the outcome of modeled burnout when adjusting pressure. This is in contrast to Figure 4-5 that shows a constant burnout at much different partial pressures of O₂ since the mole fraction of O₂ is constant for the various pressure conditions.

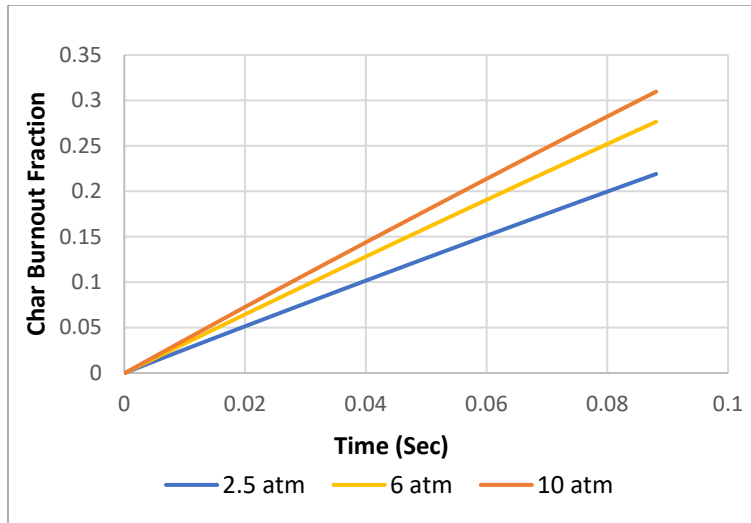


Figure 4-6: Char burnout curves for various pressures using Hurt-Calo parameters in the CCK-Oxy code

Figure 4-7 shows the particle temperature curves using the HC parameters. Similar to the char burnout curves, the particle temperatures also increase with increasing pressure at a constant mol fraction of O₂.

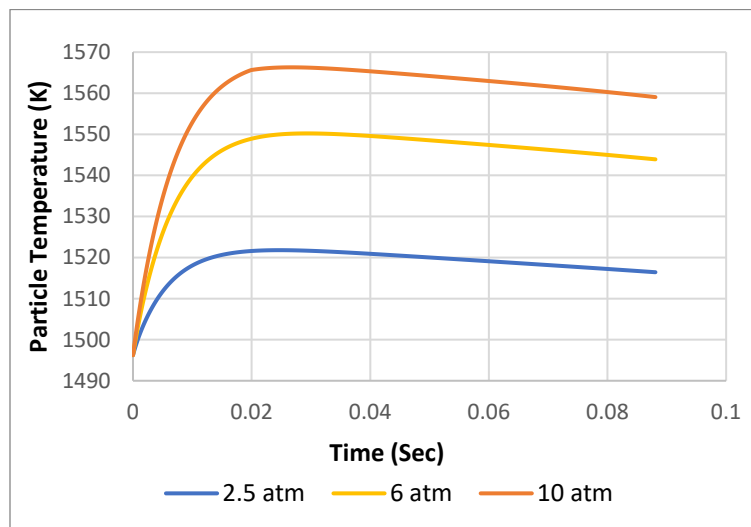


Figure 4-7: Particle Temperature curves for various pressures using Hurt-Calo parameters

4.4 χ Factor Challenges with CCK

One of the major difficulties in dealing with the model was the initial limitation of the CCK-Oxy code to replicate the physical run conditions of the DZ pressurized char oxidation data sets. The code results showed that no matter how high the pre-exponential factor (the fitting parameter) was set, the burnout could not be achieved in the amount of time specified in the experiment. This section explains the χ factor and diffusion limitations in more detail.

4.4.1 χ Factor and Combustion Zones

There are three classifications for char oxidation when considering diffusion. Zone 1 represents burning that occurs when the oxidation is controlled by the kinetics, which occurs at low temperatures. There is no limitation based on the diffusion to the particle. The particle burns consistently throughout the particle since there is O₂ available throughout the particle. The combustion is only limited by the speed of the surface mechanisms in the pores. The particle diameter will remain relatively constant during most of the burn but the density will decrease.

Zone 3 represents the opposite burning mode. This type of oxidation occurs at high temperatures when the kinetics are extremely fast and the burn rate is purely limited by how fast the O₂ can diffuse to the surface. There is no O₂ available throughout the particle and is all consumed on the exterior surface of the particle. For this reason, the density of the particle remains relatively constant but the particle shrinks during the burn.

Finally, Zone 2 is a middle ground between the previous two combustion regimes. The oxidation is partially-controlled by kinetics and partially-controlled by diffusion. Pore diffusion

plays a part in this regime. Both the density of the particle and the diameter decrease during the burn.

The χ factor is an expression that helps to quantify this concept. Shown in equation 15, this parameter is defined as the actual burn rate divided by the maximum diffusion rate. The χ factor represents the fraction of the actual burn rate compared to the maximum possible burning rate for that temperature and bulk O₂ concentration. The maximum rate is the film diffusion-controlled rate.

$$\chi = \frac{\text{Actual rate}}{\text{Max diffusion rate}} \quad (\text{Eq 15})$$

where the maximum diffusion rate can be calculated from Equation 16 assuming that $P_{O_2,s}$ is negligible:

$$n_{O_2,max}'' = k_m'' * P_{O_2,\infty} \quad (\text{Eq 16})$$

Cancelation of the diffusion terms yields an expression for χ based solely off the partial pressures of O₂ shown in equation 17:

$$\chi = 1 - \frac{P_{O_2,s}}{P_{O_2,\infty}} \quad (\text{Eq 17})$$

The χ factor ranges from 0 to 1. Low values are indicative of Zone 1 burning where the oxidation is controlled by kinetics. A high value, close to 1, is indicative of Zone 3 burning where the oxidation is controlled by diffusion. A value of 1 is an upper bound to char conversion.

Equation 17 is a simple expression for the χ factor but is not fully accurate because the diffusion terms don't actually cancel each other out unless the value of χ is 1. The diffusion term

at the maximum burning rate is larger than at the actual burning rate unless the rates are the same. If the bulk temperature is held constant, the particle and subsequent film temperatures increase which makes the diffusion term larger as well. A true expression for χ is defined in Equation 18 which would yield lower true χ values.

$$\chi = \frac{k_{m}''(P_{O_2,\infty} - P_{O_2,s})}{k_{m,T_{max}}''(P_{O_2,\infty})} \quad (\text{Eq 18})$$

4.4.2 CCK Diffusion Limitations

At each iteration in the CCK and CBK codes, the χ factor is monitored and a condition is placed on the combustion. The diffusion rate is set equal to the kinetic rate at each time step, and the surface partial pressure is calculated. When the surface kinetic rate is extremely high the surface partial pressure becomes very small and the net rate approaches the maximum diffusion rate. In the combined search for the particle temperature and surface partial pressure the χ factor may exceed 1.0, which is not a realistic solution. When the χ factor exceeds 1.0, the code restricts the net combustion rate to 99.9% of the maximum and continues with the next surface partial pressure and temperature values until convergence is achieved for both the surface partial pressure and particle temperature.

Within the CCK code, the maximum diffusion rate limitation made it impossible to replicate the Dong Zeng burn conditions. No pre-exponential factor value could produce a burn fast enough to match the burnout curve. The initial explanation was that perhaps those burn conditions were impossible. However, replicating the burn with the CBK code showed that it was possible and yielded reasonable χ factor values. The CCK code could only replicate the DZ data if the maximum diffusion restriction was taken away. Figure 4-8 shows χ factor curves

corresponding to two runs, one from the CCK code (not diffusion limited) and the other from the CBK code. These curves were both generated using conditions from the DZ data set. Noting that the maximum possible value for χ is 1, it is apparent that the CCK run seems impossible as the values start at 1.6 and descend to 1.2. However, for the same conditions and burnout, the CBK ranges from 0.8 to 0.6. This is closer to diffusion control than kinetic control but it does show that the burnout regime is physically possible. While the formulas for calculating the χ factor in both codes are the same, the inputs into those equations change. A great deal of effort was put into isolating exactly what happens differently throughout the time steps, but the most concise answer is that the kinetic models vary which solve for different surface partial pressures and temperatures to achieve the same char burnout. These partial pressures and temperatures go into calculating different maximum possible rates which affects the χ factor.

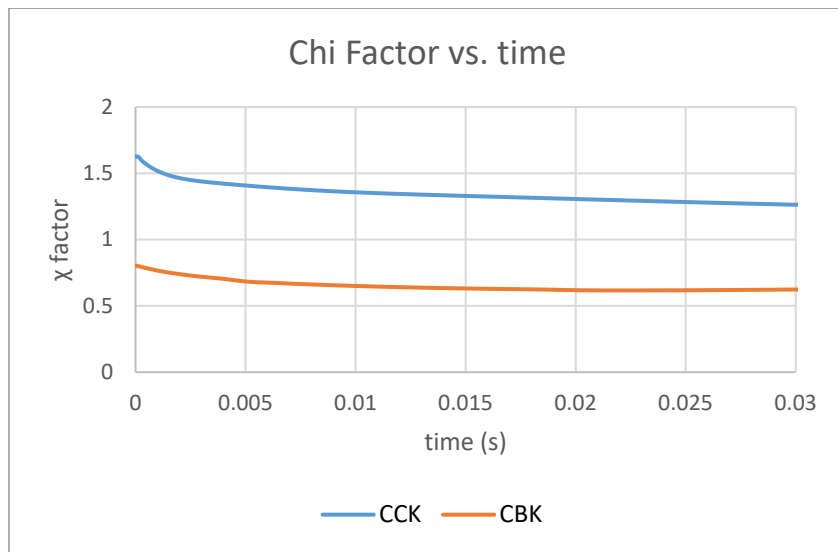


Figure 4-8: Two χ factor curves vs. time during char particle burnout that reach the same burnout fraction that matches the DZ data set for 2.5 atm at the lowest O_2 concentration.

Since the CBK could model the DZ data set conditions while considering the maximum diffusion possible, it was decided to continue with the calculations with the CCK model without the diffusion restriction. The CBK can model all the range of data that encompasses this work. Since it doesn't experience this limitation across the data set, it was assumed that this would be an acceptable assumption for the CCK modeling in this regime without exceeding the true maximum diffusion condition. The exact reason for this discrepancy is left for future work.

5. Results and Discussion

This section elaborates on the Dong Zeng data set inputs that were used for the modeling scenarios. Comparisons are drawn for the modeling results for the different models across the pressure range. Finally, a sensitivity analysis is presented for various parameters for the various pressure conditions.

5.1 Modeling Conditions

The CCK code requires the following input parameters to run the code: pressure, temperature profile, velocity profile, gas composition, residence time, collection height, coal type, diameter, and heating rate to produce char burnout. All of those parameters were extracted from the DZ data set and are presented in Tables 5-1 to 5-7. Table 5-1 shows the temperature profiles used to model the data sets in the CCK code. The CCK code receives the gas temperature profile history in the form of a 6th order polynomial. The polynomials in Table 5-1 were generated by curve-fitting the raw data from Zeng's work. Since the fit was sufficiently good with a 3rd or 2nd order polynomial and higher orders overfit the limited number of datapoints, the higher orders were left as zeros.

Table 5-1: Data Set Gas Temperature Profiles

Pressure (atm)	Gas Temperature Profile (K) as a function of distance from the burner (m)
2.5	$T_g(x) = -25701x^3 + 3556.1x^2 - 490.22x + 1459.7$
6	$T_g(x) = -606.34x^2 - 2055x + 1493.7$
10	$T_g(x) = 4240.8x^2 - 3847x + 1489.8$

The method to obtain the particle velocity data set in Table 5-2, is nearly identical to the method that was used to obtain the temperature profiles, except that the polynomials were generated from fitting points on the curves calculated from Fluent in Dong Zeng’s work.

Table 5-2: Data Set Velocity Profiles

Pressure (atm)	Velocity Profile (m/s) as a function of distance from the burner (m)
2.5	$V(x) = 81.156x^3 - 51.502x^2 + 11.227x + 0.6623$
6	$V(x) = -1024.2x^4 + 670.68x^3 - 156.53x^2 + 14.4x + 0.2132$
10	$V(x) = 8422x^5 - 6148.1x^4 + 1624.9x^3 - 187.8x^2 + 8.9742x + 0.2038$

The bulk gas compositions of the high-pressure flat-flame burner were calculated by assuming complete combustion of the feed gases listed in Zeng’s work, as shown in Table 5-3. (The columns on the left show the feed gas rate and the columns on the right show the calculated product gas compositions). One clarifying note is that a couple of the mole fractions shown in Zeng’s modeling are slightly different than what is calculated and shown in the table below. It

was decided to proceed with using values obtained from the full combustion of the reactant gases rather than the published product values.

Table 5-3: Data Set Feed Gas Rates and Product Compositions

Gas	Feed Gas Rates				Product Gas Compositions			
	CH ₄	Air	O ₂	N ₂	CO ₂	H ₂ O	O ₂	N ₂
Unit	L/min	L/min	L/min	cc/min	Mol %	Mol %	Mol %	Mol %
2.5 atm	1.74	16.55	1	150	8.95%	17.90%	5.12%	68.03%
	1.74	16.55	2	150	8.51%	17.03%	9.76%	64.70%
	1.74	16.55	3.3	150	8.00%	16.01%	15.16%	60.83%
	1.74	16.55	4.94	150	7.44%	14.88%	21.11%	56.56%
6 atm	2.16	20.5	0.7	200	9.17%	18.34%	2.91%	69.59%
	2.16	20.5	1.25	200	8.96%	17.92%	5.12%	68.00%
	2.16	20.5	2.5	200	8.52%	17.03%	9.80%	64.65%
10 atm	2.49	23.5	0.75	250	9.23%	18.45%	2.61%	69.71%
	2.49	23.5	2.9	250	8.54%	17.09%	9.80%	64.57%
	2.49	23.5	3.6	250	8.34%	16.69%	11.91%	63.05%

Table 5-4 shows the residence time and corresponding collection probe heights which were determined from the corresponding velocity profiles. The values were calculated since they were not explicitly given in Zeng's work, as described earlier in Section 4.1.2.

Table 5-4: Data Set Residence Times and Collection Probe Heights*

Pressure (atm)	Residence Time (ms)	Collection Probe Height (in)
2.5	55.7	2
6	76.4	1.25
10	44.8	0.5

*These values were calculated since they weren't explicitly given in Dong Zeng's work.

The values in Table 5-5 lists the diameter, heating rate and mode of burning. The degree of swelling and char density are obtained from subroutines in the CCK code based on the pressure, temperature, and maximum heating rate. Some of the input parameters for the CCK model are derived from the Pitt 8 coal. The proximate and ultimate analyses for the Pitt 8 coal are shown in Table 5-6.

Table 5-5: Data Set Diameter, Heating Rate, and Mode of Burning

Diameter (micron)	Heating Rate (K/s)	Mode of Burning
107.5	10^5	0.2

Table 5-6 Data Set Proximate and Ultimate Analysis-Pitt8

Proximate Analysis (wt%)			Ultimate Analysis (wt%, daf)				
Moisture (as rec'd)	Ash (dry)	VM (daf)	C	H	N	S	O
1.44%	10.72	34.34	84.58	5.47	2.00	0.49	7.44

The measured char burnout data for each O₂ concentration are shown in Table 5-7. The code generates a burnout curve and residence time is compared to the char burnout percentage.

Table 5-7: Data Set Char Burnout Data for each O₂ condition

Pressure (atm)	Gas Composition (Mol % O ₂)	Char Burnout (Wt %)
2.5	5.12%	17.02%
	9.76%	27.93%
	15.16%	51.34%
	21.11%	71.89%
6	2.91%	17.25%
	5.12%	62.19%
	9.80%	80.68%
10	2.61%	17.19%
	9.80%	30.36%
	11.91%	64.56%

5.2 Solving for the Pre-Exponential Factor

The initial pre-Exponential factor A_{30} is the only undefined kinetic parameter needed to run the CCK-Oxy code. The rest of the parameters are ratios of A_{30} and can be determined from this value (Niksa et al., 2003). They are then updated as the code proceeds. (A_{30} for example becomes A_3). Solving for A_{30} involved using graphical approach. With four guesses the value for that condition would be determined. First an educated guess was made and the code was run. Based off the modeled char burnout result a second guess was made to encompass the actual value from the data set, one above and one below. With those two values plotted and a trendline made, the root of the equation was found and was used for the third guess. The three points were

used to generate a quadratic function and the root was solved for again. This is the A_{30} value used for modeling.

While this solver method worked well for the single point solutions, the approach had to be modified slightly when solving for an A_{30} value fit from multiple data points. Instead of solving for an A_{30} value that made the error zero, a value was determined that minimized the sum squared error between the actual data points and the modeling results. This value was found by the following procedure. Three values of A_{30} were chosen in which the middle A_{30} value showed the lowest error of the three and the errors were plotted. A quadratic equation was fit to the error vs. the A_{30} values. The derivative of the quadratic equation was set to zero and the resulting solution yielded an A_{30} value for a multipoint data fit. The CCK calculations of char burnout using this value of A_{30} were performed and compared to the actual char burnout data. Since the CCK code starts with the CPD code, the time to start char oxidation starts after time zero at the end of pyrolysis. The total time of devolatilization and char oxidation were included in the data fitting.

5.3 Comparison with Char Burnout Data

Actual vs. modeled char burnout for the given conditions are compared using parity plots. An error of $\pm 2\%$ on the measured coal burnout was assumed; the resulting data error band is shown on the plots above and below the parity line. These plots show the modeled burnouts using the Hurt-Calo (HC) parameters as well as the Niksa-Hurt (NH) parameters. Comparisons were made for the 2.5, 6, and 10 atm cases. Calculations made with kinetics optimized for each individual pressure were compared as well as calculations made with a single set of kinetics for

all pressures. Since Zeng’s work provided modeled values for the combined pressure group conditions, those are compared alongside the CCK model outputs using the different kinetic parameters. All burnout data are presented as a percentage of dry, ash-free coal rather than as a percentage of the char, since that was how the data were presented in the Zeng dissertation.

5.3.1 2.5 atm Case

Figure 5-1, shows the modeling results for the 2.5 atm case for both HC and NH parameters. The first data point (measured coal burnout of 62.25% daf) was used to find the A_{30} value which yielded an exact fit for both models. This A_{30} value was then used to model the remaining data points. As seen, the next point is quite accurate but the other data points with higher O_2 exhibit more error. The HC parameters in this case however, exhibited a better fit than the NH parameters.

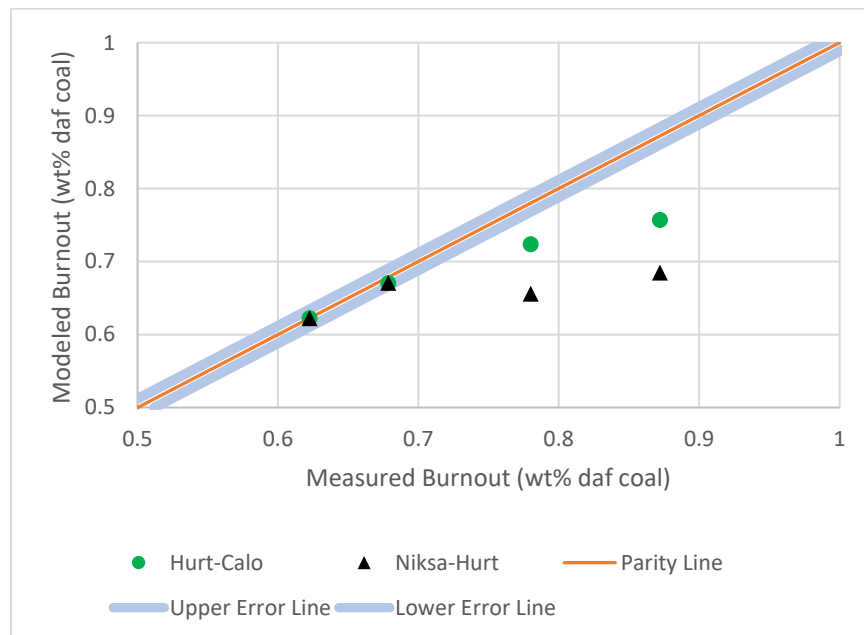


Figure 5-1: 2.5 atm single point solution parity plot

Figure 5-2 uses the 2.5 atm data set but finds a single A_{30} for all of the O_2 conditions at this pressure. In this case the HC model shows the best agreement for the first three data points but has the most error for the highest O_2 condition. The DZ model and NH show similar errors across the data range. Regardless, most of the modeling data points land near or within the error bands of the experimental data.

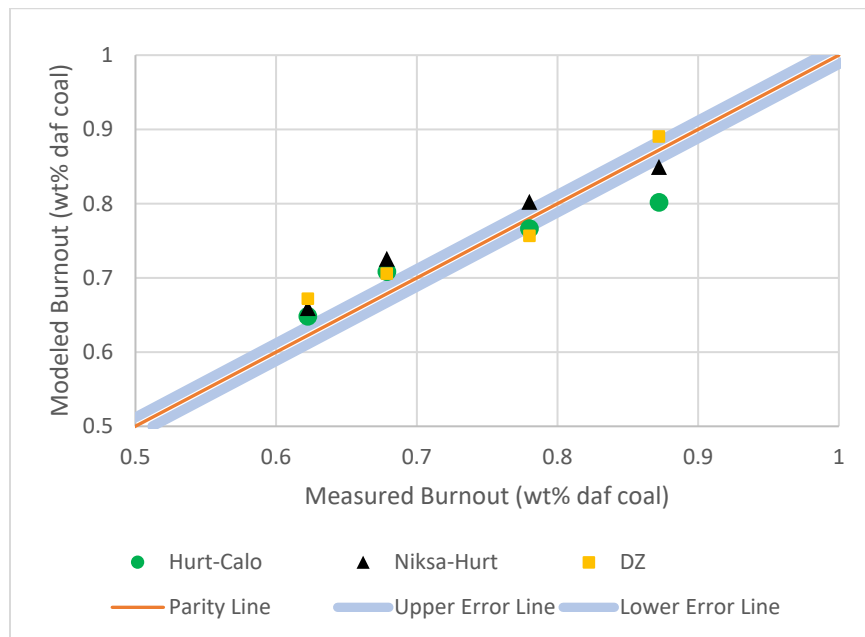


Figure 5-2: 2.5 atm all O_2 conditions solution parity plot

5.3.2 6 atm Case

Figure 5-3 shows a plot similar to Figure 5-1 where the first datapoint is used to find the A_{30} and is then used to model the remaining data points. The other two O_2 conditions in this model don't yield a good fit. The parity plot for the 6 atm group solution results are shown in figure 5-4. While the results are similar for the 3 models the CCK model using HC parameters yielded the best agreement by a small margin.

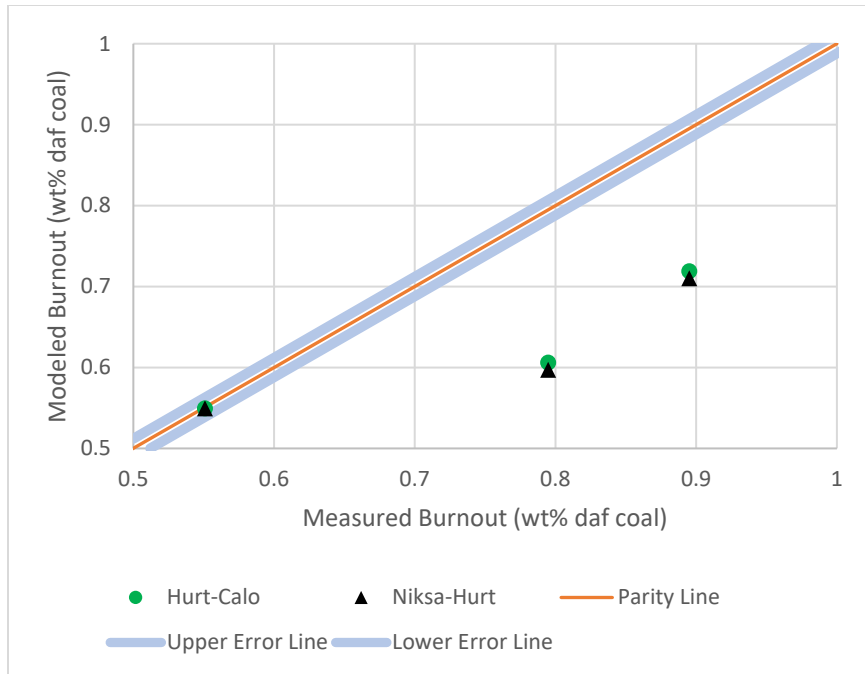


Figure 5-3: 6 atm single point solution parity plot

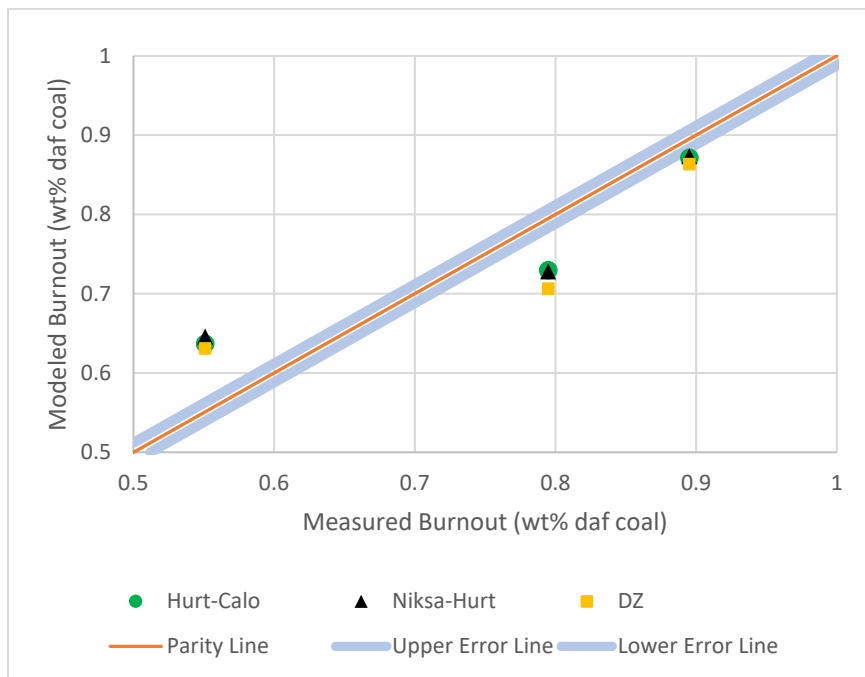


Figure 5-4: 6 atm all O₂ conditions solution parity plot

5.3.3 10 atm Case

In Figure 5-5, the parity plot of modeled vs. calculated burnout is shown for the 10 atm case. The second O₂ condition shows fairly good agreement by modeling it with the pre-exponential factor from the first, but the third condition shows a fair amount of error. For the group solve condition shown in Figure 5-6, there is similar agreement between the models, but the Zeng model actually yields the best agreement in this case by a small margin.

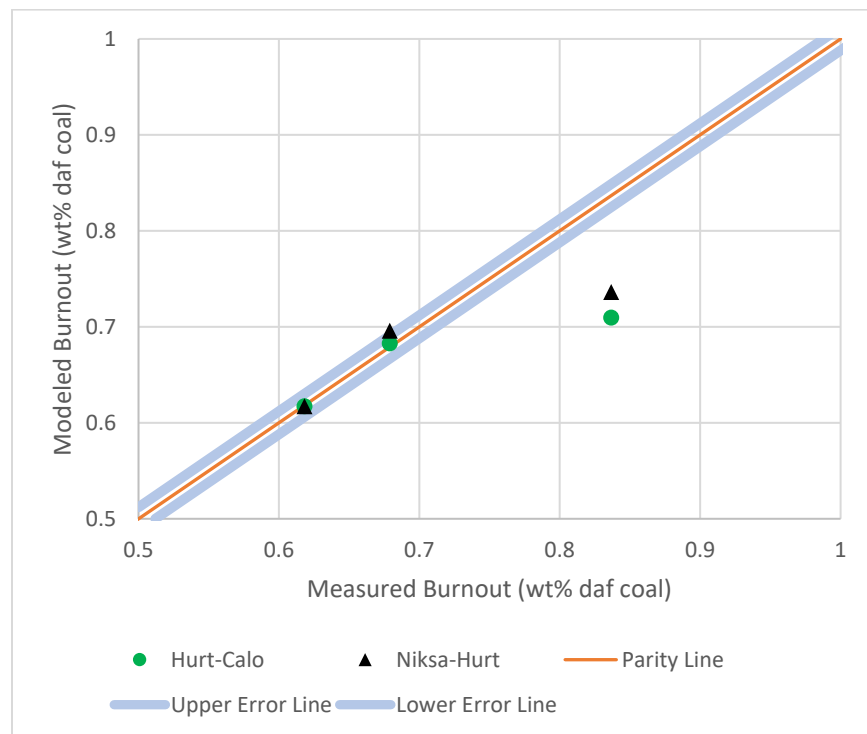


Figure 5-5: 10 atm single point solution parity plot

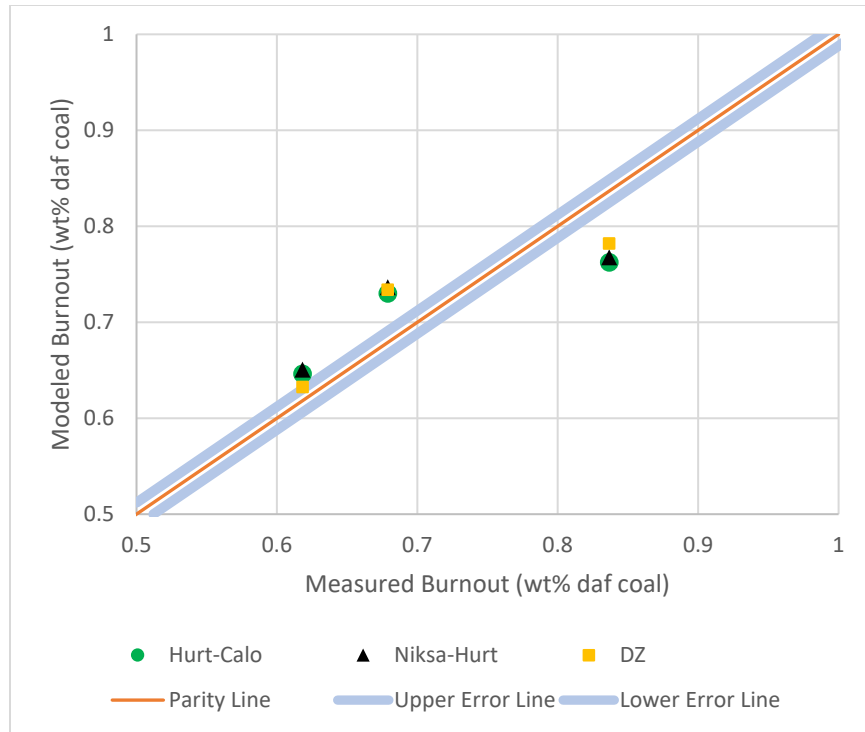


Figure 5-6: 10 atm all O_2 conditions solution parity plot

5.3.4 Group Solve

The next set of figures were generated by solving for a pre-exponential factor using all of the O_2 conditions for all pressures simultaneously. The corresponding numerical data is shown in Table 5-8. Figure 5-7 shows the comparison of this solution for both the HC and NH parameters. Visually it is hard to say which approach performed better. Statistical comparisons are provided in section 5.3.5.

Figure 5-8 uses the same data from Figure 5-7 for HC, but also compares this to all of the individual pressure modeling runs for HC as well to show the difference in error. For most of the data points there isn't a significant difference but some calculations differ by 5 wt%.

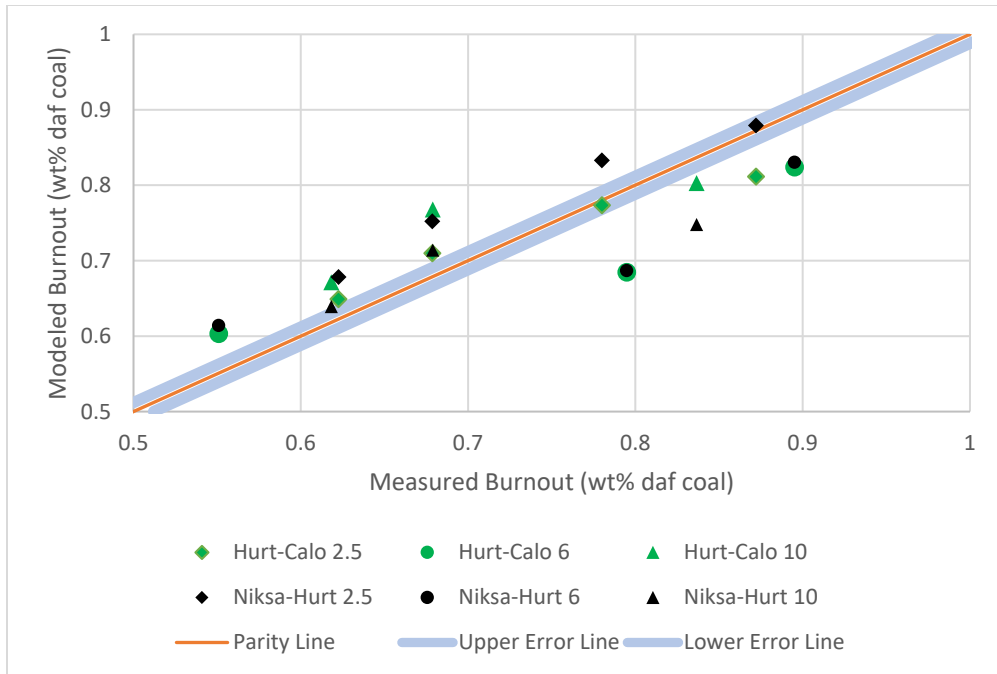


Figure 5-7: Parity plot generated using all available data and solving for an A_{30} for both Hurt-Calo and Niksa-Hurt Parameters.

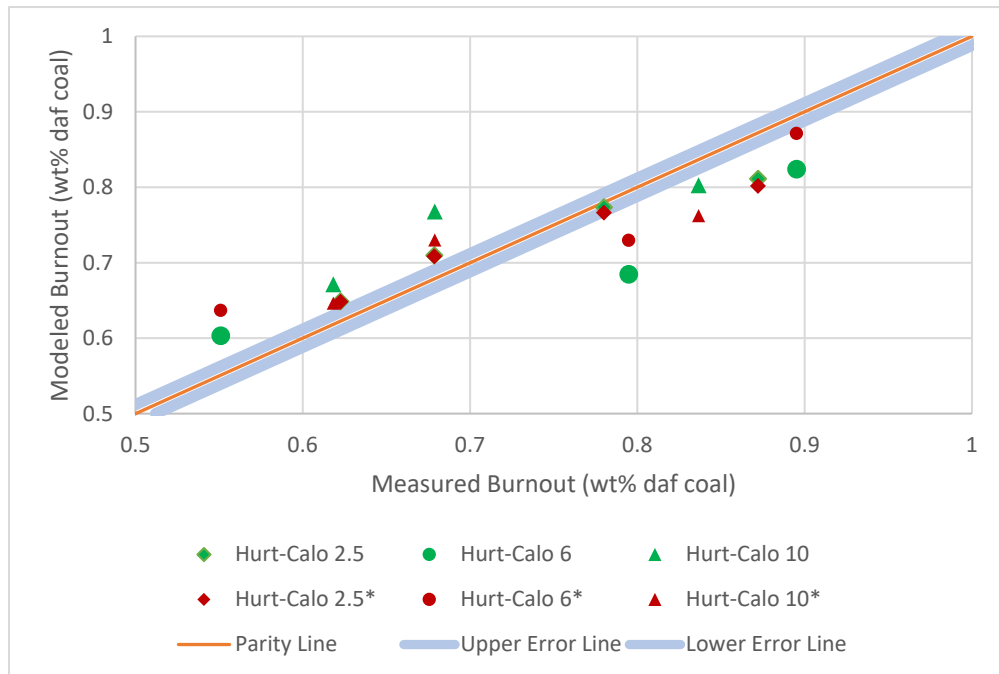


Figure 5-8: Parity plot generated using all available data from each pressure group using Hurt-Calo parameters and solving for A_{30} . (The * denotes the pressure group solutions).

5.3.5 Statistical Comparison

The data from many of the charts are listed in Table 5-8, showing the percent error for each char burnout condition for various models. The full data set is shown in Appendix C in Table C-1 and Table C-2. Columns 3 to 5 in Table 5-8 show the char burnout modeling results compared to the actual data when using a single pressure condition A_{30} value for the 3 different kinetic models (Dong Zeng (DZ), Niksa-Hurt (NH), and Hurt Calo (HC)). DZ uses the CBK code while NH and HC use the CCK code. Columns 5 and 6 both show the modeling results generated using the HC kinetic parameters. Column 5 uses a single pressure condition A_{30} value whereas column 6 uses the entire data set to solve for A_{30} . The average of the errors and averages of the absolute errors are shown.

Figure 5-9 shows a graphical representation of the absolute error data in Tables 5-8, C-1, and C-2 with a box and whisker plot. The results are grouped by how much data was used to generate the A_{30} value for the various modeling runs (most to least from left to right). More charts are shown in Appendix C. Using all the data to generate the fitting parameter and modeling the cases yielded an absolute average error of 7-8% with HC showing a half percent improvement over NH (as denoted by the “x” in the charts). Another finding is that the lowest absolute average errors are found by A_{30} values from data grouped at each pressure (between 6-7%). The absolute error is lowest for the DZ, HC, and NH data labeled “Each Pressure” in that order. The HC and NH in this group show two dots outside the box and whisker plots. Since those points are more than 1.5 times the width of the inner quartile range box for those sets, they are classified as outliers so the extending whisker doesn’t encompass them.

Table 5-8: Various Model Comparison Data

Pressure	Gas O ₂ Composition	Dong Zeng (Each Pressure)	Niksa-Hurt (Each Pressure)	Hurt-Calo (Each Pressure)	Hurt-Calo (All Pressures)
atm	Mol %	% Error	% Error	% Error	% Error
2.5	5.12%	-7.95%	-5.93%	-4.16%	-4.25%
	9.76%	-4.02%	-6.96%	-4.42%	-4.61%
	15.16%	-2.11%	-2.88%	1.74%	0.83%
	21.11%	2.98%	2.59%	8.06%	6.97%
	Average	-2.78%	-3.29%	0.30%	-0.26%
	Absolute Avg.	4.27%	4.59%	4.59%	4.16%
6	2.91%	-14.54%	-17.28%	-15.61%	-9.53%
	5.12%	11.12%	8.40%	8.17%	13.85%
	9.80%	3.53%	2.42%	2.65%	7.93%
	Average	0.04%	-2.16%	-1.59%	4.08%
	Absolute Avg.	9.73%	9.37%	8.21%	10.43%
10	2.61%	-2.31%	-5.24%	-4.56%	-8.61%
	9.80%	-8.10%	-8.48%	-7.55%	-13.11%
	11.91%	6.51%	8.24%	8.86%	4.04%
	Average	-1.30%	-1.83%	-1.08%	-5.89%
	Absolute Avg.	5.64%	7.32%	6.99%	8.59%
All	Average	-1.49%	-2.51%	-0.68%	-0.65%
	Absolute Avg.	6.32%	6.84%	6.58%	7.37%

Another significant finding can be seen from the last 4 data sets on the chart that compare HC and NH modeling error when the A₃₀ value is solved for using a single O₂ value at each pressure or a single O₂ and single pressure. These 4 sets show that HC outperforms NH in these categories by an average of ~2%. In other words, HC is better at extrapolating from one condition to other O₂ and pressure conditions. Also, the last 4 modeling cases were all single point solutions, so the first data point has no error as denoted by the bottom bar extending to zero for those runs.

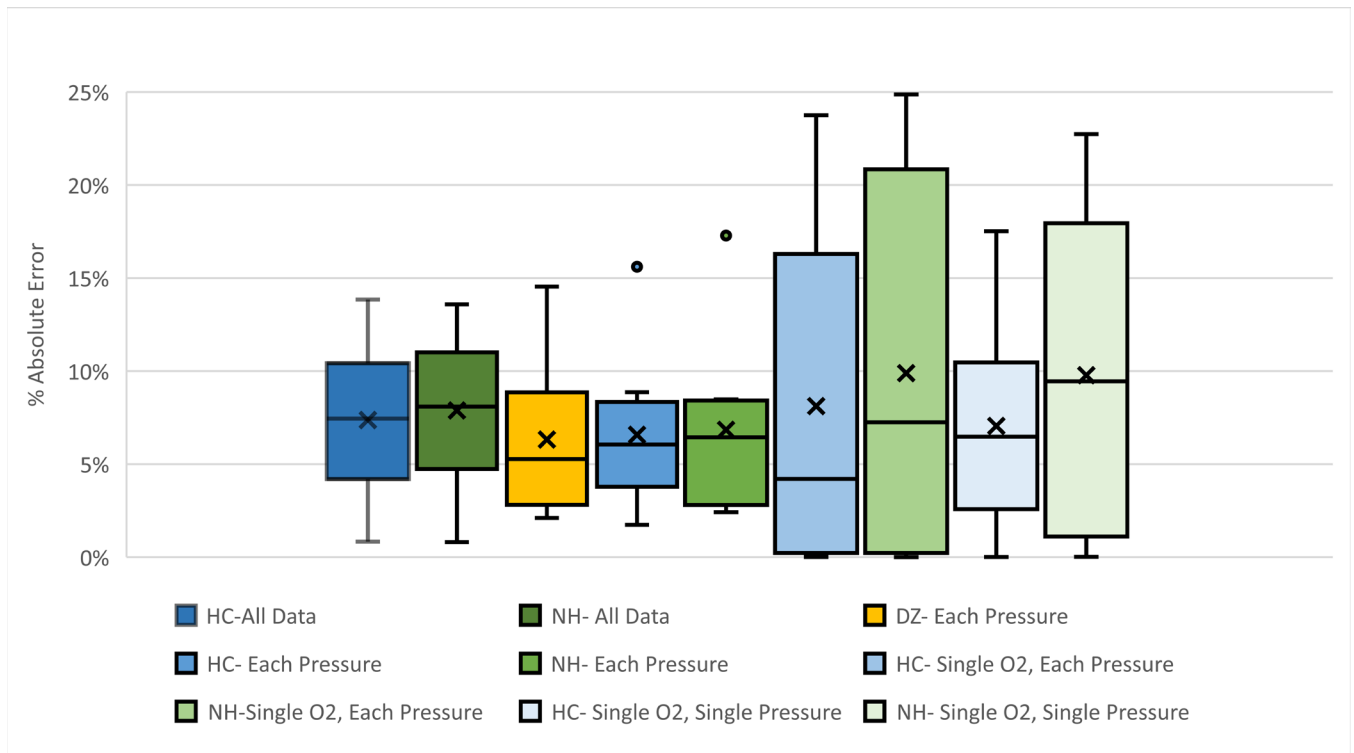


Figure 5-9: Absolute Error Statistical Comparison-All Modeling Methods

Table 5-9 shows the pre-exponential factors (A_{30}) that were determined for the various group solution modeling attempts from Table 5-8. The single point solutions are shown in Appendix C. It is interesting to note the optimized A_{30} value for each pressure reaches a peak in the 6 atm case for both the HC and NH models. Zeng's (2005) modeling showed the same trend for both the high and low temperature data taken as a function of pressure. When taking all other pressure factors into account such as swelling, diffusivity, surface kinetics, there is something about that pressure that yields a higher pre-exponential factor. That would likely indicate that something is not well understood about either the surface mechanism around that pressure range, or perhaps the formation of the char in that range yields a reactivity that is higher which requires the higher pre-activation energy in this solver method. Note that the A_{30} values used for the HC

and NH models differ by nine orders of magnitude; other kinetic parameters in each model compensate.

Table 5-9: Pre-exponential Factors from Modeling

Pressure (atm)	All O ₂ at a Pressure		All O ₂ for all Pressures	
	Hurt-Calo (sec ⁻¹)	Niksa-Hurt (sec ⁻¹)	Hurt-Calo (sec ⁻¹)	Niksa-Hurt (sec ⁻¹)
2.5	2.85×10 ¹⁸	8.15×10 ⁹	6.31×10 ¹⁸	9.50×10 ⁹
6	1.05×10 ¹⁹	1.69×10 ¹⁰		
10	3.78×10 ¹⁸	1.40×10 ¹⁰		

5.3.6 Summary

The various methods described in this section had varying degrees of success. Solving for an A₃₀ value using one pressure-O₂ condition and then using that value to compare other scenarios had mixed results. Detailed results of the modeling are shown in Table-5-8, Figure 5-9, and various other tables and figures in Appendix C. While the CCK-Oxy model was able to do a great job modeling some of the data points to within a few percent (which is within the assumed error bars of the measurements), others were up to 20% off. However, considering all the potential errors from data collection to modeling subroutines this is still quite good. Using Hurt-Calo instead of Niksa-Hurt parameters performed better generally especially when extrapolating between pressures (not fitting the A₃₀ parameter with data between pressures).

Fitting a kinetic parameter with a single O₂ and single pressure (5.12% O₂ and 2.5 atm) and using it to model many pressures and O₂ concentrations resulted in large error. Using a

single O₂ (the lowest) at each pressure performed slightly worse. This was surprising. It is possible that the single O₂ and single pressure condition chosen just happened to be a good fit. The best results for modeling used all of the O₂ conditions within a pressure are used to solve for an A₃₀ value. This was the approach taken by Zeng. Using all of the data together which gives a single value for the entire series shows only a minor increase in the average absolute error for the data set.

There are a few possible explanations for the error in these findings. One explanation for the error when extrapolating data between pressures is that something about the pressure itself affects the formation of the char and consequently the reactivity, while the reactivity used for modeling stays the same across cases. Since devolatilization at different pressures affects what molecules are released from the coal and in what bond configurations, then it could be reasonably assumed that the actual reactivity would be different. There is one study that looks into what may cause the difference in reactivity with char formed at pressure (Krishnamoorthy et al., 2019). Though not a perfect comparison since they study gasification, they show that the intrinsic rate was less affected by char generation pressure and that the apparent reaction rate was primarily dependent on surface area evolution during the gasification process. There is still however error with using one O₂ condition to solve for A₃₀ and extrapolating within a pressure condition. Each of the submodels has some associated error. Submodels such as the kinetic mechanism and associated parameters, the annealing model, the swelling model, or the pore diffusion model each contribute to the modeling uncertainty.

5.4 Sensitivity Analysis

A sensitivity analysis was performed by varying key parameters and the corresponding change in char burnout. The following parameters were varied: total pressure, partial pressure, gas composition, gas temperature, diameter, and pre-exponential factor. Table 5-10 shows the base case conditions and also shows the range over which those conditions are varied. Since the primary purpose of this thesis is pressure, all of the listed parameters are varied alongside pressure and not each one compared to all of the others. All of the cases generated were carried out to 70 ms to show an equal time comparison one to another. This time frame was chosen since as parameters are varied between the selected ranges, modeled char burnout yielded a decent spread that was at least 5% and not higher than 95%.

Table 5-10: Sensitivity Analysis Parameter Base Case and Range

Parameter	Basis	Range	Units
Total Pressure	5	2.5 - 10	(atm)
Partial Pressure O ₂	0.125 (2.5 atm, 5% O ₂)	0.0625 - 1.0	(atm)
Mol percent O ₂	5%	0.625% - 40%	(%)
Mol percent CO ₂	0%	0 - 95%	(%)
Gas Temperature	1500	1300 - 1700	(K)
Diameter	107.5	50 - 150	(μm)
Kinetic Parameter A _{3o}	6.31×10^{18}	2.847×10^{18} - 1.05×10^{19}	(sec ⁻¹)

The first section below deals with sensitivity to the total pressure and O₂ partial pressure and contains results from both the Hurt-Calo (HC) and Niksa-Hurt (NH) models. The rest of the sections that change other parameters explore the sensitivity effects with just the HC model.

5.4.1 Total Pressure and O₂ Partial Pressure

Both total pressure (P_T) and O₂ partial pressure (P_{O_2}) have an effect on the overall char burnout. Varying both P_{O_2} and P across different ranges also changed the O₂ mole fraction (y_{O_2}). This section shows how burnout was affected by changing P_T and P_{O_2} for both HC and NH parameters used in the CCK code. Figure 5-10 shows calculations where P was varied from 2.5 to 10 atm and P_{O_2} was varied from 0.0625 to 1 atm. This set of calculations was performed at a constant A_{3o} and so formation effects at these pressures were not considered. The corresponding percentages of O₂ ranged from 0.625 to 40 mol%. Each partial pressure or pressure step was doubled from one to another. This way the increasing one step in both partial pressure and total pressure yielded the same mole fraction of O₂.

For each of the pressure series (denoted by a different color in Figure 5-10), char burnout increased as the partial pressure of O₂ increased. However, for each of these partial pressures, increasing total pressure decreased overall char burnout and acted as a hindrance in the overall burnout process. Total pressure is inversely proportional to diffusion so increasing the total pressure decreases the diffusivity and hence mass transfer rate of O₂ through the particle boundary layer. For each P_{O_2} group, increasing P_T also has the effect of lowering y_{O_2} .

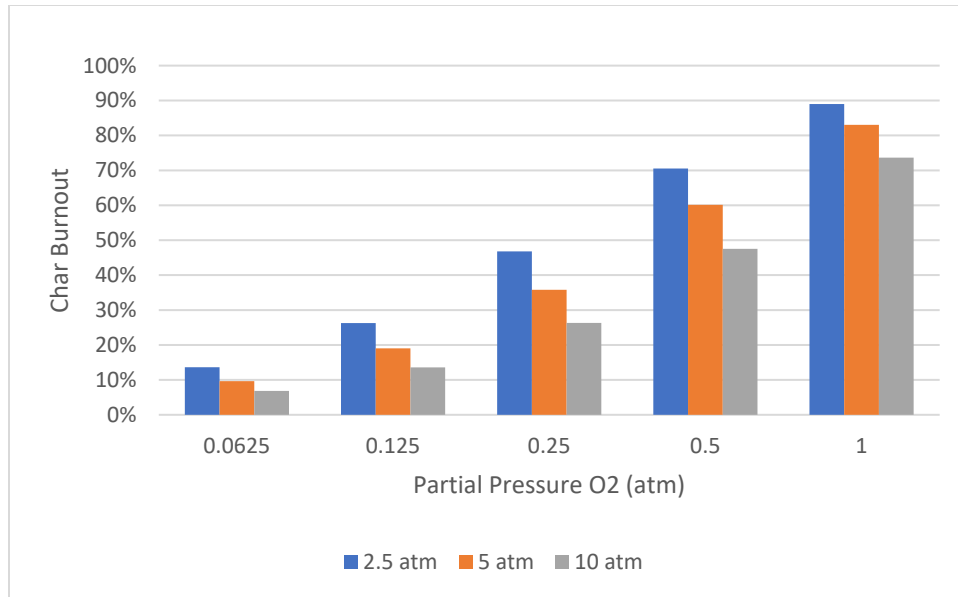


Figure 5-10: Char burnout vs. total pressure and partial pressure using the CCK code with the Hurt-Calo model.

Figure 5-11 shows the same information as Figure 5-10 but the results were generated using NH parameters. In this case, there is a much larger spread in burnout when P_T was varied for a given P_{O_2} , indicating a more severe hindrance of the reaction with increasing pressure than with HC parameters. For example, for $P_{O_2} = 0.25$ atm burnout changed from 47% to 26% using the HC parameters but from 58% to 23% using the NH parameters.

Figure 5-12 shows some of the same data from the two previous figures arranged differently. While Figures 5-10 and 5-11 show burnouts with varying y_{O_2} conditions, Figure 5-12 shows selected data that is all at a fixed value of y_{O_2} . Increasing P_T at fixed y_{O_2} shows an increase in char burnout (due to an increase in P_{O_2}). The HC model showed more sensitivity to P_T than the NH model at $y_{O_2} = 0.05$. For the NH model, the values are almost independent of P_T and P_{O_2} and the changes are almost all due to y_{O_2} . Doubling or quadrupling P_{O_2} as long as y_{O_2} stayed the same resulted in almost no effect.

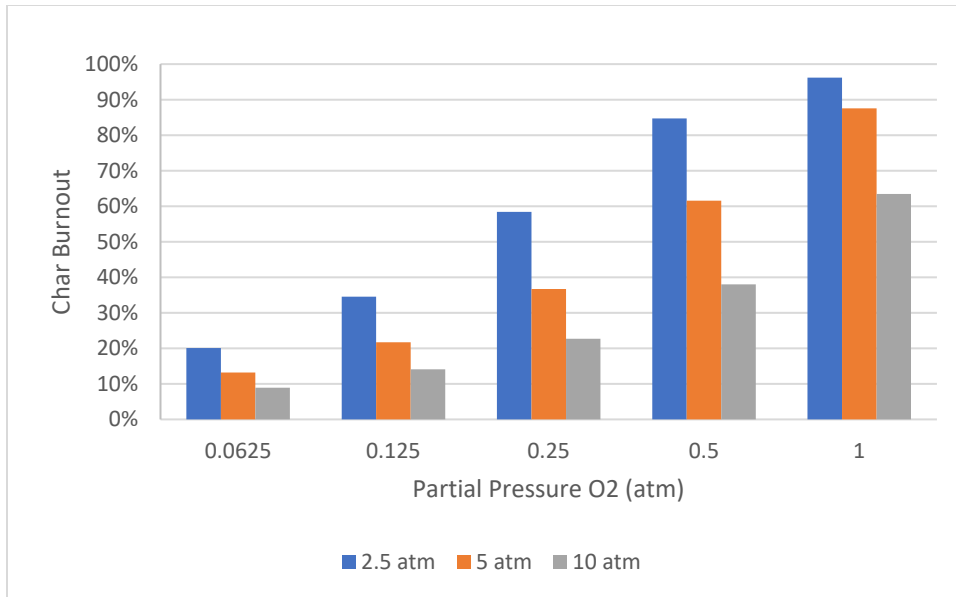


Figure 5-11: Char burnout vs. total pressure and partial pressure using the CCK code with the Niksa-Hurt model.

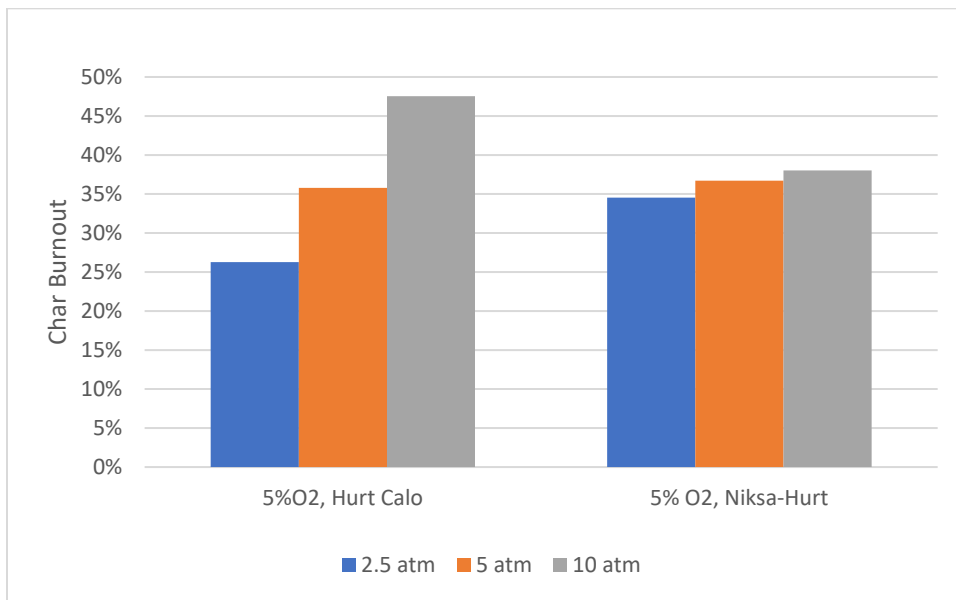


Figure 5-12: Comparison of char burnout at 5% O₂ for various pressures and 2 kinetic models

Figures 5-13 and 5-14 illustrate this same principle for the NH and HC models, respectively. Burnout curves are shown for P_T and P_{O2} combinations, noting the y_{O2} values. Note

that the char burnout fraction starts after time zero because devolatilization time is taken into effect. Table 5-11 shows the key to the legends for those charts; the color of the lines in Figures 5-13 and 5-14 represent the different y_{O_2} values, and the line types represent the different values of P_T .

Table 5-11: Legend explanation for Figures 5-13 and 5-14

P =	2.5 atm	5 atm	10 atm
2.5% O₂	0.0625 atm O ₂	0.125 atm O ₂	0.25 atm O ₂
5% O₂	0.125 atm O ₂	0.25 atm O ₂	0.5 atm O ₂
10% O₂	0.25 atm O ₂	0.5 atm O ₂	1.0 atm O ₂

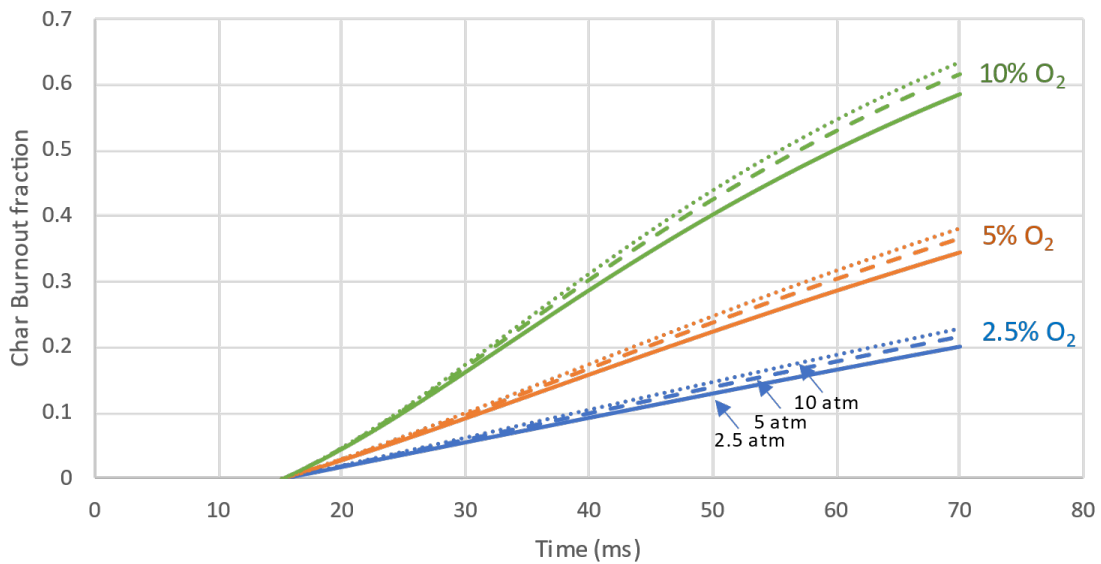


Figure 5-13: Burnout curves for various pressure- O_2 combinations using the Niksa-Hurt model.

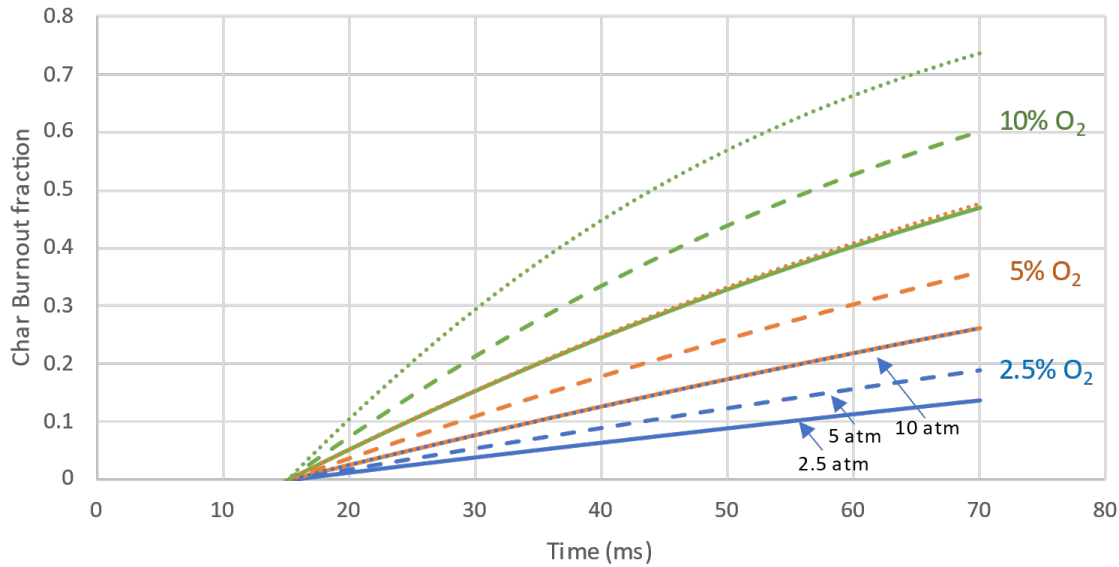


Figure 5-14: Burnout curves for various pressure- O_2 combinations using the Hurt-Calo model.

Both Figures 5-13 and 5-14 show that increasing y_{O_2} and P_{O_2} increases char burnout. However, it is clear, from the two preceding figures that using the HC parameters result in a much larger change in burnout due to y_{O_2} and P_{O_2} . One thing of note in Figure 5-13 is that a couple of the runs nearly overlap (for example, the 2.5% O_2 , 10 atm curve overlaps the 5% O_2 , 2.5 atm curve). These are not at the same partial pressure or the same mole fraction (in the example, P_{O_2} 's of 0.25 and 0.125 atm, respectively). It is clear that use of the HC parameters results in independent effects of both y_{O_2} and P_{O_2} , while use of the NH parameters indicated that y_{O_2} was the only factor affecting char burnout.

Another important thing to point out is that the work in this section up to this point was all completed using the same kinetic parameters, but as shown in Table 5-9, pressure seems to have an effect on the best-fit pre-exponential factor for each pressure. The left-hand side of Figure 5-15 shows the effects of pressure when taking into account the different best-fit A_{30} values. Using different A_{30} values generated at the different pressure conditions in the code

produced the highest burnout at 5 atm. This trend has also been observed in various other investigations. One study showed that surface rates increased with pressure up to 5 atm and a further increase in pressure led to a decrease in the reaction rate (MacNeil and Basu, 1998). Another study, while it was a gasification study, exhibited a similar behavior showing an apparent reactivity maximum at ~6 atm and decreased with increasing pressure however intrinsic reactivity stayed the same (Krishnamoorthy et al., 2019). Zeng et al. (2005) measured TGA char-O₂ reactivities at the char formation pressures for chars generated in a high pressure flat-flame burner. Zeng noted that the activation energy determined reached a minimum at 6 atm, meaning that the reactivity peaked at 6 atm. The trend shown on the left-hand side of Figure 5-15 is consistent with the findings cited here. (Note: like Figure 5-12, the char burnouts modeled in Figure 5-15 were at a fixed y_{O₂} contrary to the values shown in Figures 5-10 and 5-11 which shows that increasing pressure inhibits char oxidation rate).

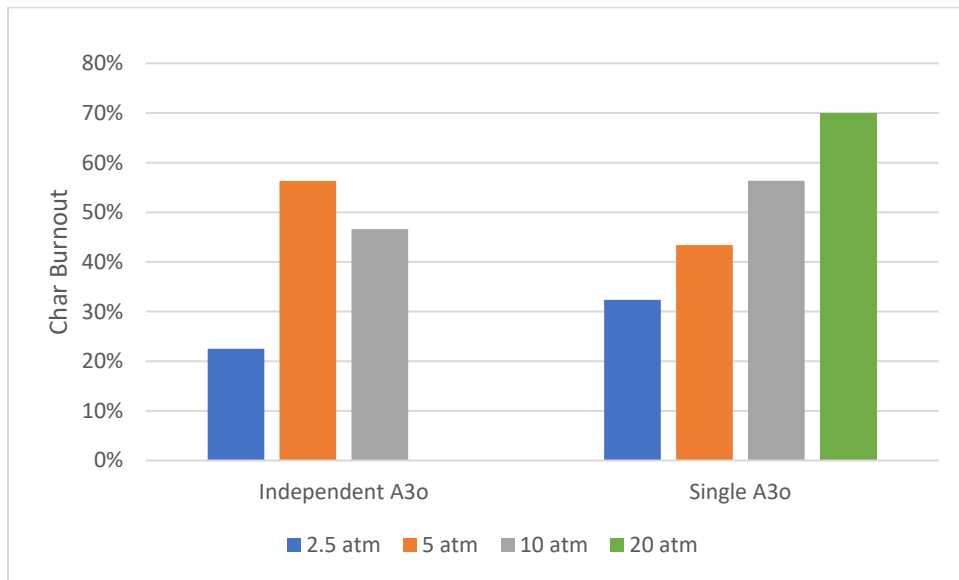


Figure 5-15: Char burnout bar charts at various pressures and fixed 5 mole % O₂ for two separate kinetic approaches using the Hurt-Calo model.

Using the global pre-exponential factor (i.e, the A_{30} from curve-fitting data from all of the pressures) indicated that burnouts increased as pressure increased in all cases (see right-hand side of Figure 5-15), which is not consistent with the left-hand side of Figure 5-15. Based on these findings and the findings in the literature cited in the previous paragraph, it appears that the effects of pressure during char formation and the resulting changes in reactivity seem to maximize around 5-6 atm.

5.4.2 CO₂ Gas Composition

Burnout is not only affected by the O₂ concentration, but also the composition of the surrounding environment, though to a much smaller extent. For example, replacing the N₂ background with CO₂ changes the diffusivity and thermal conductivity of the gas. Figure 5-16 shows burnout curves for 0%, 50%, and 95% CO₂, with 5% being O₂ and the remainder N₂ across 3 pressures.

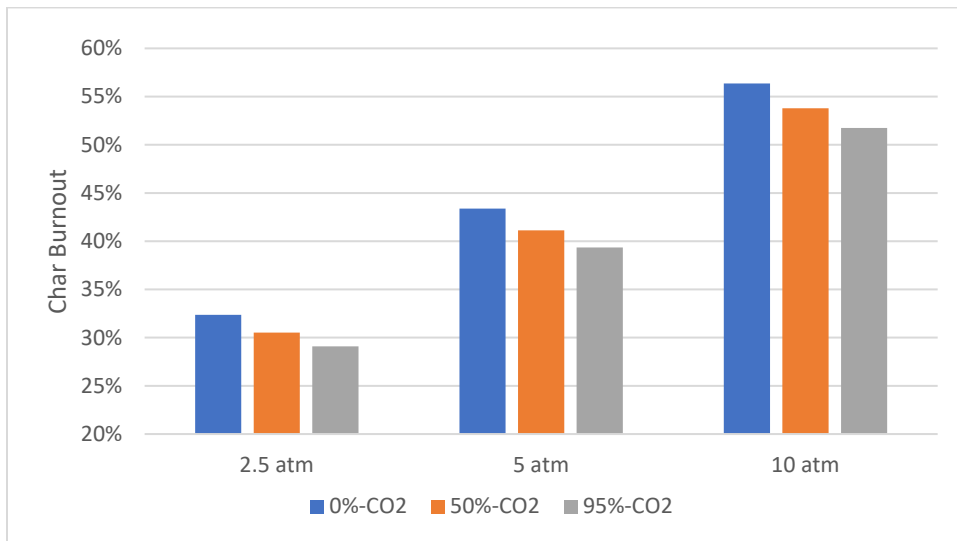


Figure 5-16: CO₂ effects on char burnout at various pressures

The common trend is that CO₂ inhibits the burnout overall by limiting the mass transfer rate of O₂. However, the decrease in burnout due to the presence of CO₂ is much less than the effect of changing the total pressure (y_{O_2} was held constant at 5% in these calculations). Figure 5-16 is strictly looking at the effects of diffusion because formation effects and gasification reactions were not considered in these particular calculations.

5.4.3 Gas Temperature

Gas temperature also plays a role at these burnout conditions. Figure 5-17 shows the effects of gas temperature on char burnout for various pressures. Intuitively, as gas temperature increases, burnout increases for all pressure conditions.

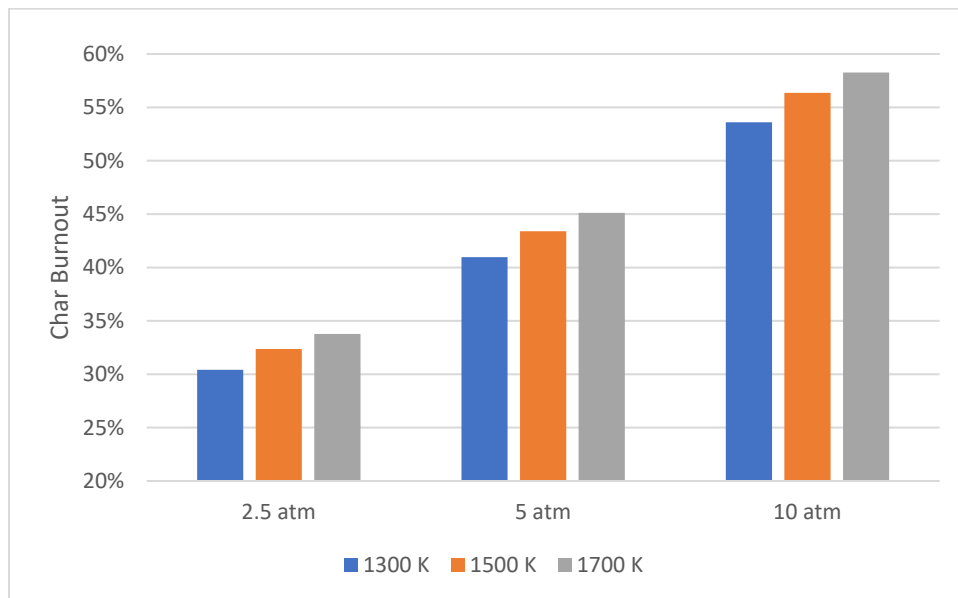


Figure 5-17: Gas Temperature effects on char burnout at various pressures

However, the effect at these conditions is not that significant in comparison to the change in pressure and the accompanying change in partial pressure. One reason that the change is not that significant is because the burnout is at a relatively high χ factor. This means that diffusion of O_2 through the particle boundary layer is playing a significant part. Temperature has a much larger effect when the reaction is mainly kinetically-limited. The effect in that case would be exponential as opposed to being proportional to the two-thirds power.

5.4.4 Diameter

Diameter plays a significant role in char burnout modeling. Figure 5-18 shows the effects of diameter changes across various pressures. Decreasing the diameter exhibits a large change in modeled char burnout fraction and that difference gets larger as the diameter decreases.

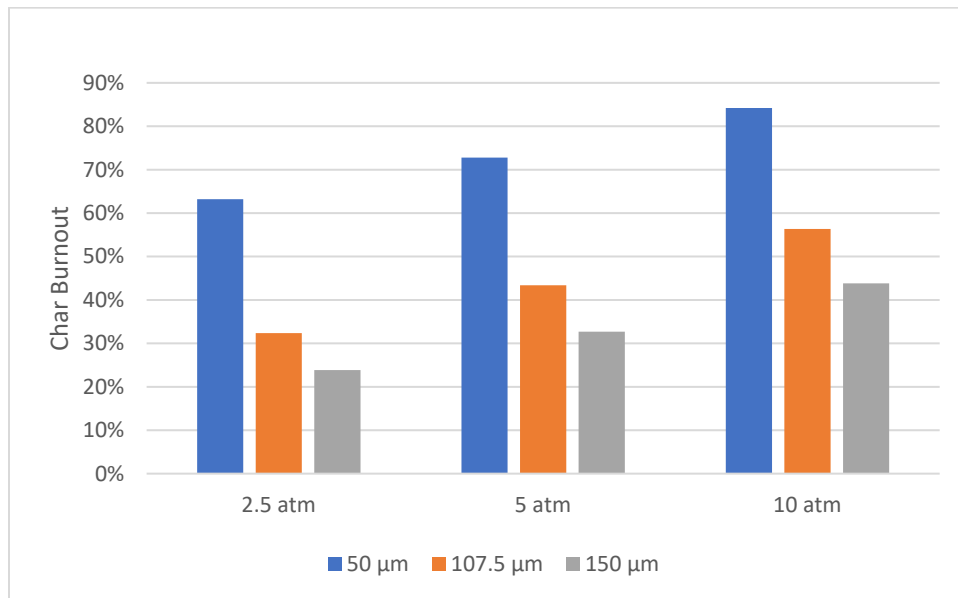


Figure 5-18: Particle diameter effects on char burnout at various pressures

The difference also gets less pronounced as pressure increases. At larger particle diameters, the

mass transfer coefficient decreases since $k_m'' = \frac{Sh \cdot D_{O_2}}{d_p}$.

5.4.5 Pre-exponential Factor

Changing the pre-exponential factor (A_{30}) creates a significant change on char burnout.

Figure 5-19 shows that the kinetic parameter variation changes the char burnout by a fairly significant degree. The trend is similar across pressures. Three A_{30} values were chosen from the data fit values at the various pressure conditions to be representative of the change to the A_{30} due to pressure formation. A change in coal type would also have a large effect on A_{30} .

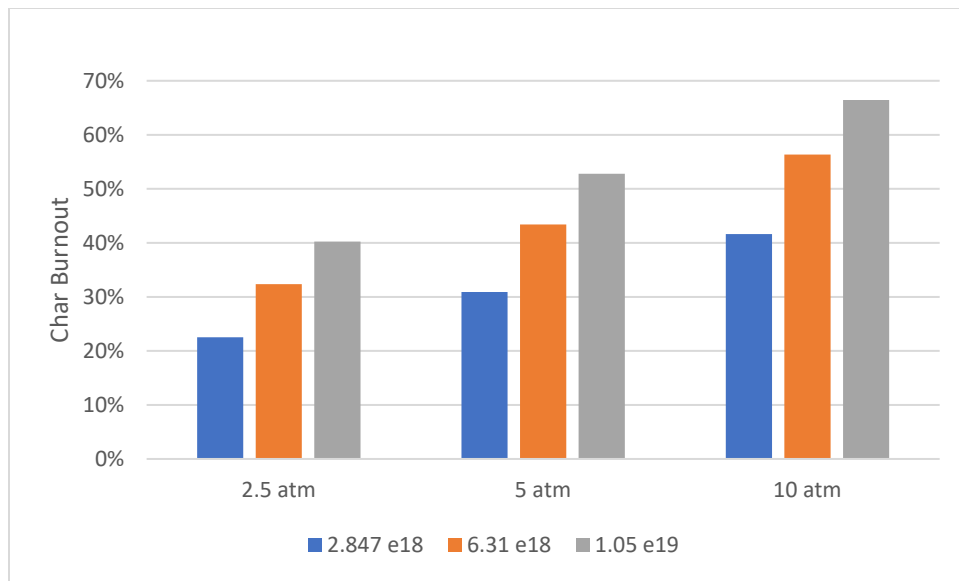


Figure 5-19: A_{30} effects on char burnout at various pressures

5.4.6 Summary

The parameters that were varied in this section produced varying effects on the modeled char burnouts. Adjusting P_{O_2} or y_{O_2} had the greatest impact, with changing the diameter in second. Adjusting P_T or A_{30} was about half the impact of the first two. Adjusting gas temperature and mol% CO_2 had a relatively minimal impact at these conditions. Increasing P_T , P_{O_2} , y_{O_2} , gas temperature, or A_{30} all increased char burnout while increasing diameter or mole fraction CO_2 had the opposite effect. Table 5-12 shows the exact numbers from these modeling cases.

Table 5-12: Sensitivity Analysis Results

Parameter	Units	Change	Effect on Char burnout
Total Pressure	(atm)	2.5 to 10	+23.3%
Partial Pressure O_2	(atm)	0.0625 to 0.5	+56.9%
Mol percent O_2	(%)	2.5% to 20%	
Mol percent CO_2	(%)	0 to 95	- 4.0%
Gas Temperature	(K)	1300 to 1700	+4.2%
Diameter	(μm)	50 to 150	- 40.0%
Kinetic Parameter A_{30}	(sec^{-1})	1e18 to 1.5e19	+21.4%

6. Summary and Conclusions

The high-pressure, high-heating rate data set generated by Zeng (2005) was studied to determine char oxidation rate coefficients. It was necessary to solve for the sampling locations and residence times using the original CBK code since these locations were not included in Zeng's dissertation. These data sets were modeled using the CCK code with different sets of kinetic parameters, since the CCK code included many improvements to the CBK code. A comparison was made with the original Dong Zeng (DZ) data modeling and the new CCK methods. A sensitivity analysis was performed for various parameters using the CCK model with updated kinetic parameters. The following conclusions were drawn:

- Modeling efforts with the CCK model yielded similar results to the modeling efforts of Zeng. Modeling all O₂ conditions for each pressure yielded the best fits. The Hurt-Calo (HC) parameters slightly outperformed the Niksa-Hurt (NH) parameters in modeling the group solutions (0.25-2%) and significantly outperformed in the single point solutions (2-5%). HC parameter improvements are manifest when extrapolating across pressures. Using one kinetic parameter to solve for the entire data set (A₃₀) yielded a 1% reduction in average error compared to the solutions from each individual pressure condition.

- Using HC parameters shows a change in reaction order across a realistic combustion temperature range (300K to 2000K) that goes from 0 to 1 whereas the NH parameters stays at a value of 1 for any reasonable combustion regime. With the same pre-exponential factor value there is no perceptible difference in burnout curves when changing pressure from 2.5 atm to 10 atm but there are differences when using the HC parameters. Finally, modeling char burnout with NH parameters doesn't show a significant effect of partial pressure of O₂. Changes in mole fraction of O₂ are the only major factor. With HC parameters both partial pressure and mole fraction of O₂ play a part across the pressure range. However, after fitting parameters for both models, resulting changes in calculated burnout for the DZ data were smaller than expected.
- The sensitivity analysis provided valuable insight for modeling char burnout. For the ranges selected for the parameter variation the results breakdown into three tiers. The first tier which has the most significant effect on char burnout was mole fraction or partial pressure of O₂ and particle diameter. The second tier which has about half the effect of the first tier is comprised of total pressure and the A₃₀ pre-exponential factor. The third tier which has about one-tenth of the effect of the first tier were CO₂ mole fraction and gas temperature (over the range examined). The detailed results are shown in Table 5-12. Increasing any of these parameters resulted in an increase in char burnout except diameter and CO₂ mole fraction.
- Beyond the pressure effects that are captured in the code such surface reaction, swelling, and diffusion, there appears to be an effect on the reactivity of the char. This could be due to the composition of the molecules remaining after

devolatilization, the formation of the char that remains, or the evolution of the surface area throughout combustion. The results showed a peak in reactivity at 6 atm relative to the results at 2.5 atm and 10 atm as evidenced by the pre-exponential factors in Table 5-9. This peak in reactivity seems to be consistent with some of the data in the literature.

7. Recommendations

The findings of this work resulted in further questions that could be ascertained by future work. The following recommendations remain:

- Generating more high-pressure, high-temperature, high-heating rate, entrained-flow data for various coal types, diameters, CO₂ environments and perhaps at additional pressures for further model validation. Create conditions that vary across the 3 zones of burning.
- With a larger char data set at various pressures, more certainty could be placed on the peak reactivity observed around 5-6 atm. With these data, perhaps a model could be developed linking char reactivity to the formation pressure. This may mean data from a single condition could model the breadth of pressure-temperature combinations.
- Further numerical methods that work with the solver method in the code tailored to the Nth order model may result more reliable solutions without the code crashing.
- A detailed review of diffusion limitations within the CCK and CBK codes is needed. Models can predict the same char burnout with many combinations of surface partial pressure and particle temperature with a different kinetic model. In other words, the char burnout could be accurate but the internal variables may be

incorrect that go into calculating parameters like the χ factor. Finding a way to have increased fidelity about the actual values of particle temperature and surface partial pressure would be useful.

- A more robust solver method for determining the optimum A_{30} values may yield lower error for the solutions in the CCK code since each was generated with a 4-point graphical solution.

References:

- Bai, Y., P. Wang, L. Yan, C. Liu, F. Li and K. Xie, "Effects of CO₂ on gas evolution and char structure formation during lump coal pyrolysis at elevated pressures," *Journal of Analytical and Applied Pyrolysis*, **104**, 202–209 (2013).
- Banin, V., R. Moors and B. Veefkind, "Kinetic study of high-pressure pulverized coal char combustion: experiments and modelling," *Fuel*, **76**(10), 945-949 (1997).
- Baxter, L., A. Baxter and S. Burt, "Cryogenic CO₂ capture as a cost-effective CO₂ capture process," *26th Annual International Pittsburgh Coal Conference 2009, PCC 2009*, **1** (2009).
- Croiset, E., C. Mallet, J.-P. Rouan and J.-R. Richard, "The influence of pressure on char combustion kinetics," *Symposium (International) on Combustion*, **26**(2), 3095-3102 (1996).
- EIA, "U.S. electricity generation by energy source," U.S. Energy Information Administration, <https://www.eia.gov/tools/faqs/faq.php?id=427&t=3> (2021).
- Essenhigh, R. H. and A. M. Mescher, "Influence of pressure on the combustion rate of carbon," *The Combustion Institute*, (1996).
- Fletcher, T. H., A. R. Kerstein, R. J. Pugmire, M. S. Solum and D. M. Grant, "Chemical percolation model for devolatilization. 3. Direct use of carbon-13 NMR data to predict effects of coal type," *Energy & Fuels*, **6**(4), 414-431 (1992).
- Gale, T. K., C. H. Bartholomew and T. H. Fletcher, "Decreases in the swelling and porosity of bituminous coals during devolatilization at high heating rates," *Combustion and Flame*, **100**(1), 94-100 (1995).
- Geier, M., C. R. Shaddix, K. A. Davis and H. S. Shim, "On the use of single-film models to describe the oxy-fuel combustion of pulverized coal char," *Applied Energy*, **93**, 675-679 (2012).
- Grant, D. M., R. J. Pugmire, T. H. Fletcher and A. R. Kerstein, "Chemical model of coal devolatilization using percolation lattice statistics," *Energy & Fuels*, **3**(2), 175-86 (1989).
- Hao, T., J. Zhang, Y. Wu, J. Lu and G. Yue, "Pressure and temperature effects on the structural characteristics of coal char," **36**, 1303-1309 (2016).
- Harris, D. J. and J. H. Patterson, "Use of Australian bituminous coals in IGCC power generation technologies," *Aust Inst Energy J*, **13**, 22-32 (1995).
- Haugen, N., B. Loong and R. Mitchell, "Numerical approaches for thermochemical conversion of char," *Progress in Energy and Combustion Science*, **91**, 100993 (2022).
- Hecht, E. S., C. R. Shaddix, M. Geier, A. Molina and B. S. Haynes, "Effect of CO₂ and steam gasification reactions on the oxy-combustion of pulverized coal char," *Combustion and Flame*, **159**(11), 3437-3447 (2012).

- Hecker, W. C., P. M. Madsen, M. R. Sherman, J. W. Allen, R. J. Sawaya and T. H. Fletcher, "High-pressure intrinsic oxidation kinetics of two coal chars," *Energy & Fuels*, **17**(2), 427-432 (2003).
- Hendrickson, T. A., Synthetic fuels data handbook, Denver, CO (1975).
- Holland, T., S. Bhat, P. Marcy, J. Gattiker, J. Kress and T. H. Fletcher, "Modeling effects of annealing on coal char reactivity to O₂ and CO₂, based on preparation conditions," *Energy & Fuels*, (2017).
- Holland, T. and T. H. Fletcher, "Comprehensive model of single particle pulverized coal combustion extended to oxy-coal conditions," *Energy & Fuels*, **31**, 2722-2739 (2017).
- Holland, T. M., "A comprehensive coal conversion model extended to oxy-coal conditions," Ph.D. Dissertation, Chemical Engineering, Brigham Young University (2017).
- Hong, J., "Modeling char oxidation as a function of pressure using an intrinsic langmuir rate equation," Chemical Engineering, Brigham Young University (2000).
- Hong, J., W. C. Hecker and T. H. Fletcher, "Modeling high-pressure char oxidation using langmuir kinetics with an effectiveness factor," *Proceedings of the Combustion Institute*, **28**(2), 2215-2223 (2000).
- Hurt, R., J.-K. Sun and M. Lunden, "A kinetic model of carbon burnout in pulverized coal combustion," *Combustion and Flame*, **113**(1-2), 181-197 (1998).
- Hurt, R. H. and J. M. Calo, "Semi-global intrinsic kinetics for char combustion modeling," *Combustion and Flame*, **125**(3), 1138-1149 (2001).
- Krishnamoorthy, V., N. Krishnamurthy and S. Pisupati, "Intrinsic gasification kinetics of coal chars generated in a high-pressure, high-temperature flow reactor," *Chemical Engineering Journal*, **375**, 122028 (2019).
- Lasek, J., M. Janusz, J. Zuwała, K. Głód and A. Iluk, "Oxy-fuel combustion of selected solid fuels under atmospheric and elevated pressures," *Energy*, **62**, 105-112 (2013).
- Lei, M., C. Sun and C. B. Wang, "The crystal structure of coal char and the mineral transformation of coal ash during coal conversion under pressurized conditions," *Ranliao Huaxue Xuebao/Journal of Fuel Chemistry and Technology*, **46**, 925-933 (2018).
- Liu, G. S. and S. Niksa, "Coal conversion submodels for design applications at elevated pressures. Part II. Char gasification," *Progress in Energy and Combustion Science*, **30**(6), 679-717 (2004).
- Ma, J., "Soot Formation During Coal Pyrolysis," Chemical Engineering, Brigham Young University (1996).
- Ma, L. and R. Mitchell, "Modeling char oxidation behavior under Zone II burning conditions at elevated pressures," *Combustion and Flame*, **156**(1), 37-50 (2009).
- MacNeil, S. and P. Basu, "Effect of pressure on char combustion in a pressurized circulating fluidized bed boiler," *Fuel*, **77**(4), 269-275 (1998).

- Mathias, J. A., "High pressure oxidation rates for large particles," M.S. Thesis, Brigham Young University (1996).
- Monson, C. R., G. J. Germane, A. U. Blackham and L. Douglas Smoot, "Char oxidation at elevated pressures," *Combustion and Flame*, **100**(4), 669-683 (1995).
- Niksa, S., G.-s. Liu and R. H. Hurt, "Coal conversion submodels for design applications at elevated pressures. Part I. devolatilization and char oxidation," *Progress in Energy and Combustion Science*, **29**(5), 425-477 (2003).
- Pang, L., Y. Shao, W. Zhong and H. Liu, "Experimental study and modeling of oxy-char combustion in a pressurized fluidized bed combustor," *Chemical Engineering Journal*, **418**, 129356 (2021).
- Ranish, J. M. and P. L. Walker, "High pressure studies of the carbon-oxygen reaction," *Carbon*, **31**(1), 135-141 (1993).
- Shaddix, C. R. and A. Molina, "Particle imaging of ignition and devolatilization of pulverized coal during oxy-fuel combustion," *Proceedings of the Combustion Institute*, **32**(2), 2091-2098 (2009).
- Shurtz, R., "Effects of pressure on the properties of coal char under gasification conditions at high initial heating rates," Chemical Engineering, Brigham Young University (2011).
- Shurtz, R. C., K. K. Kolste and T. H. Fletcher, "Coal swelling model for high heating rate pyrolysis applications," *Energy & Fuels*, **25**(5), 2163-2173 (2011).
- Shurtz, R. C., J. W. Hogge, K. C. Fowers, G. S. Sorensen and T. H. Fletcher, "Coal swelling model for pressurized high particle heating rate pyrolysis applications," *Energy & Fuels*, **26**(6), 3612-3627 (2012).
- Shurtz, R. C. and T. H. Fletcher, "Coal char-CO₂ gasification measurements and modeling in a pressurized flat-flame burner," *Energy & Fuels*, **27**(6), 3022-3038 (2013).
- Smoot, D. L. and P. J. Smith, Coal combustion and gasification, New York, Plenum Press (1985).
- Tahmasebi, A., K. Maliutina and J. Yu, "Impact of pressure on the carbon structure of char during pyrolysis of bituminous coal in pressurized entrained-flow reactor," *Korean Journal of Chemical Engineering*, **36** (2018).
- Yang, H., S. F. Li, T. H. Fletcher and M. Dong, "Simulation of the swelling of high-volatile bituminous coal during pyrolysis," *Energy & Fuels*, **28**(11), 7216-7226 (2014).
- Ying, Z., X. Zheng and G. Cui, "Pressurized oxy-fuel combustion performance of pulverized coal for CO₂ capture," *Applied Thermal Engineering*, **99** (2016).
- Yu, J., D. Harris, J. Lucas, D. Roberts, H. Wu and T. Wall, "Effect of pressure on char formation during pyrolysis of pulverized coal," *Energy & Fuels*, **18** (2004).

- Zeng, D., "Effects of pressure on coal pyrolysis at high heating rates and char combustion," Ph.D. Dissertation, Chemical Engineering, Brigham Young University (2005).
- Zeng, D., M. Clark, T. Gunderson, W. C. Hecker and T. H. Fletcher, "Swelling properties and intrinsic reactivities of coal chars produced at elevated pressures and high heating rates," *Proceedings of the Combustion Institute*, **30**(2), 2213-2221 (2005).
- Zhang, W., Y. Zhao, S. Sun, D. Feng and P. Li, "Effects of pressure on the characteristics of bituminous coal pyrolysis char formed in a pressurized drop tube furnace," *Energy & Fuels*, **33**(12), 12219-12226 (2019).
- Zygourakis, K., "Effect of pyrolysis conditions on the macropore structure of coal-derived chars," *Energy & Fuels*, **7**(1), 33-41 (1993).

Appendix A: CCK Code

The CCK code files are posted on <https://github.com/dgundersen-1/CCK>. The development history of the code is posted in Table 2-1. Troy Holland (2017) converted these files from FORTRAN 77 to MATLAB and made his additions to the code in MATLAB. The simulations and data fitting for this project were also completed in MATLAB. Further details of the code development and history are documented elsewhere ((Fletcher et al., 1992); (Grant et al., 1989); (Hurt et al., 1998); (Liu and Niksa, 2004); (Niksa et al., 2003); (Shurtz et al., 2011); (Shurtz and Fletcher, 2013); (Shurtz, 2011; Shurtz et al., 2012)).

Appendix B: Atmospheric Flat Flame Burner Data

A significant amount of work was performed in the lab to create reasonable O_2 and T_g conditions in the FFB, as well as repeatable char oxidation data. Burning conditions (i.e., flow rates of O_2 , CO , CO_2 , and H_2) were developed for oxy-fuel conditions. Stable flames were not achieved in fuel-lean conditions until the fuel and oxidizer lines were switched.

Data points were taken for Black Thunder coal varying between 1200-1800 K in 12% excess O_2 . Initially it was difficult to achieve repeatable results, so many of the feeding system parts and collection system pieces were modified or replaced. The post modification batch of data shows more promising results, as can be seen by comparing Figures B-1 and B-2. Both sets were taken at an adiabatic flame temperature of 1450K and 12% excess O_2 .

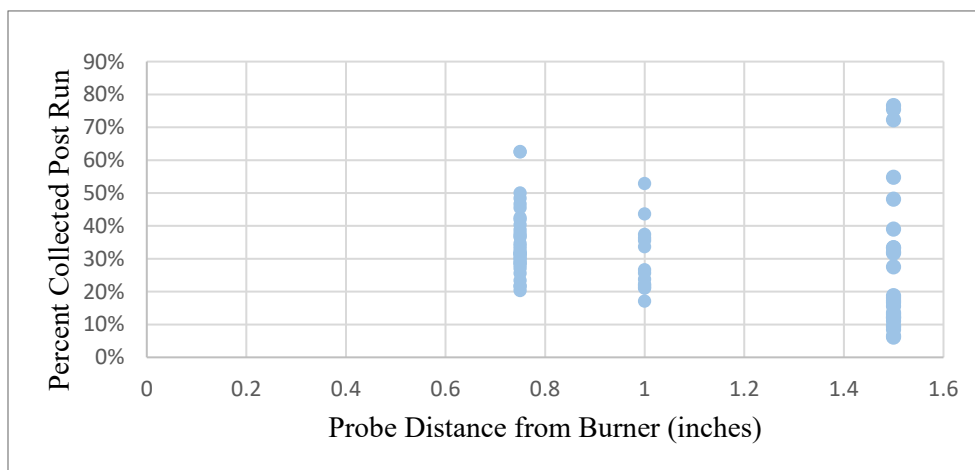


Figure B-1: Generated Black Thunder Coal Mass Conversion Data Prior to Lab Corrections at 1450 K adiabatic flame temperature

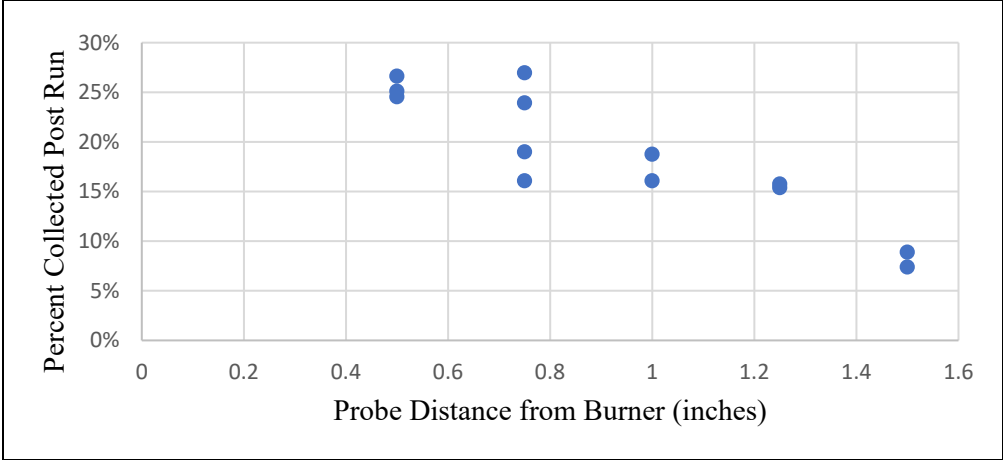


Figure B-2: Generated Black Thunder Coal Mass Conversion Data after Lab Corrections at 1450 K adiabatic flame temperature

Appendix C: Additional Data

Table C-1: Various Model Comparison Data (Group Solutions)

Pressure	Gas O ₂ Composition	Dong Zeng (Individual Pressures)	Niksa- Hurt (Individual Pressures)	Niksa-Hurt (All Pressures)	Hurt-Calo (Individual Pressures)	Hurt-Calo (All Pressures)
atm	Mol %	% Error	% Error	% Error	% Error	% Error
2.5	5.12%	-7.95%	-5.93%	-8.96%	-4.16%	-4.25%
	9.76%	-4.02%	-6.96%	-10.85%	-4.42%	-4.61%
	15.16%	-2.11%	-2.88%	-6.78%	1.74%	0.83%
	21.11%	2.98%	2.59%	-0.81%	8.06%	6.97%
	Average	-2.78%	-3.29%	-6.85%	0.30%	-0.26%
	Absolute Avg.	4.27%	4.59%	6.85%	4.59%	4.16%
6	2.91%	-14.54%	-17.28%	-11.48%	-15.61%	-9.53%
	5.12%	11.12%	8.40%	13.58%	8.17%	13.85%
	9.80%	3.53%	2.42%	7.22%	2.65%	7.93%
	Average	0.04%	-2.16%	3.11%	-1.59%	4.08%
	Absolute Avg.	9.73%	9.37%	10.76%	8.21%	10.43%
10	2.61%	-2.31%	-5.24%	-3.40%	-4.56%	-8.61%
	9.80%	-8.10%	-8.48%	-5.18%	-7.55%	-13.11%
	11.91%	6.51%	8.24%	10.60%	8.86%	4.04%
	Average	-1.30%	-1.83%	0.67%	-1.08%	-5.89%
	Absolute Avg.	5.64%	7.32%	6.40%	6.99%	8.59%
All	Average	-1.49%	-2.51%	-1.60%	-0.68%	-0.65%
	Absolute Avg.	6.32%	6.84%	7.89%	6.58%	7.37%

Table C-2: Various Model Comparison Data (Single Point Solutions)

Pressure	Gas O ₂ Composition	Hurt-Calo (Single O ₂ at each Pressure)	Niksa-Hurt (Single O ₂ at each Pressure)	Hurt-Calo (5.12% O ₂ -2.5 atm extended to all scenarios)	Niksa-Hurt (5.12% O ₂ -2.5 atm extended to all scenarios)
atm	Mol %	% Error	% Error	% Error	% Error
2.5	5.12%	-0.01%	0.00%	0.01%	0.02%
	9.76%	1.19%	1.12%	0.86%	1.29%
	15.16%	7.21%	15.90%	-4.86%	-12.30%
	21.11%	13.19%	21.45%	-9.63%	-15.60%
	Average	5.40%	9.62%	-3.41%	-6.65%
	Absolute Avg.	5.40%	9.62%	3.84%	7.30%
6	2.91%	0.25%	0.25%	4.66%	0.57%
	5.12%	23.75%	24.87%	-17.51%	-22.74%
	9.80%	19.67%	20.64%	-12.99%	-18.08%
	Average	14.56%	15.26%	-8.62%	-13.42%
	Absolute Avg.	14.56%	15.26%	11.72%	13.80%
10	2.61%	0.13%	0.13%	-3.15%	-6.60%
	9.80%	-0.59%	-2.51%	8.73%	-2.63%
	11.91%	15.17%	11.98%	-8.08%	-17.90%
	Average	4.91%	3.20%	-0.83%	-9.04%
	Absolute Avg.	5.30%	4.88%	6.65%	9.04%
All	Average	8.00%	9.38%	-4.20%	-9.40%
	Absolute Avg.	8.12%	9.89%	7.05%	9.77%

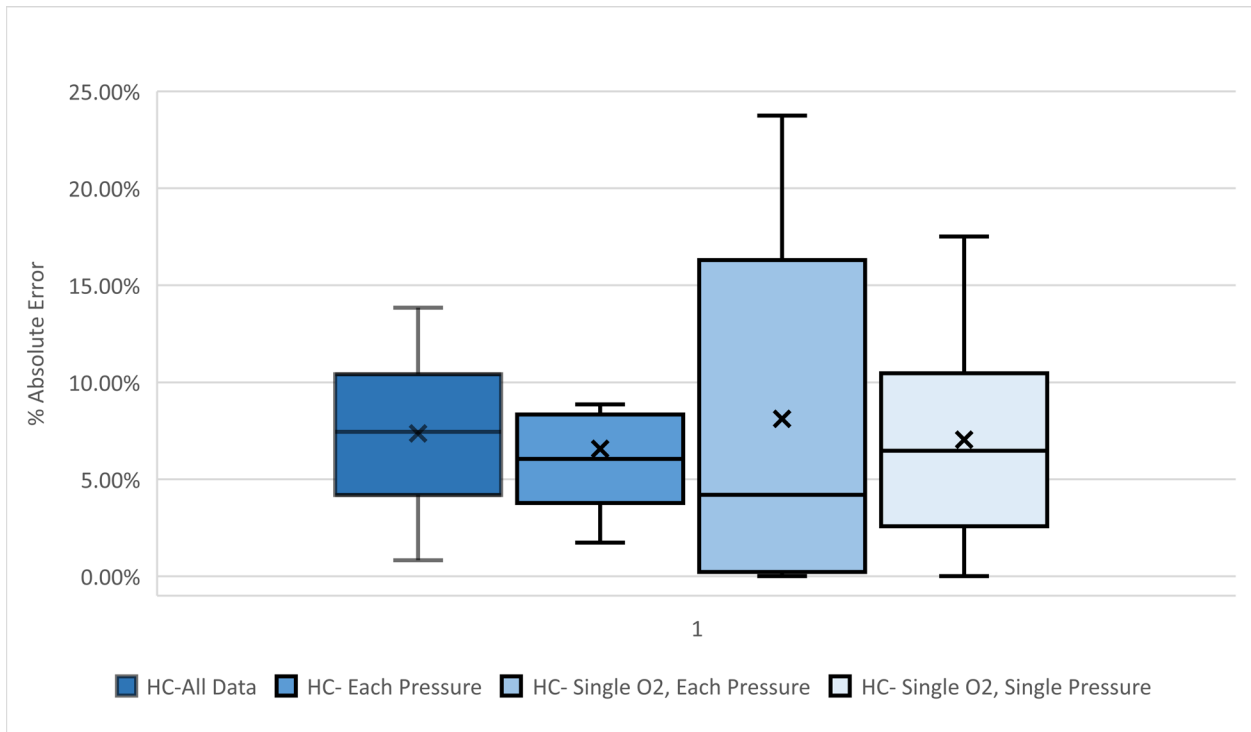


Figure C-1: Absolute Error Statistical Comparison using all Hurt-Calo modeling

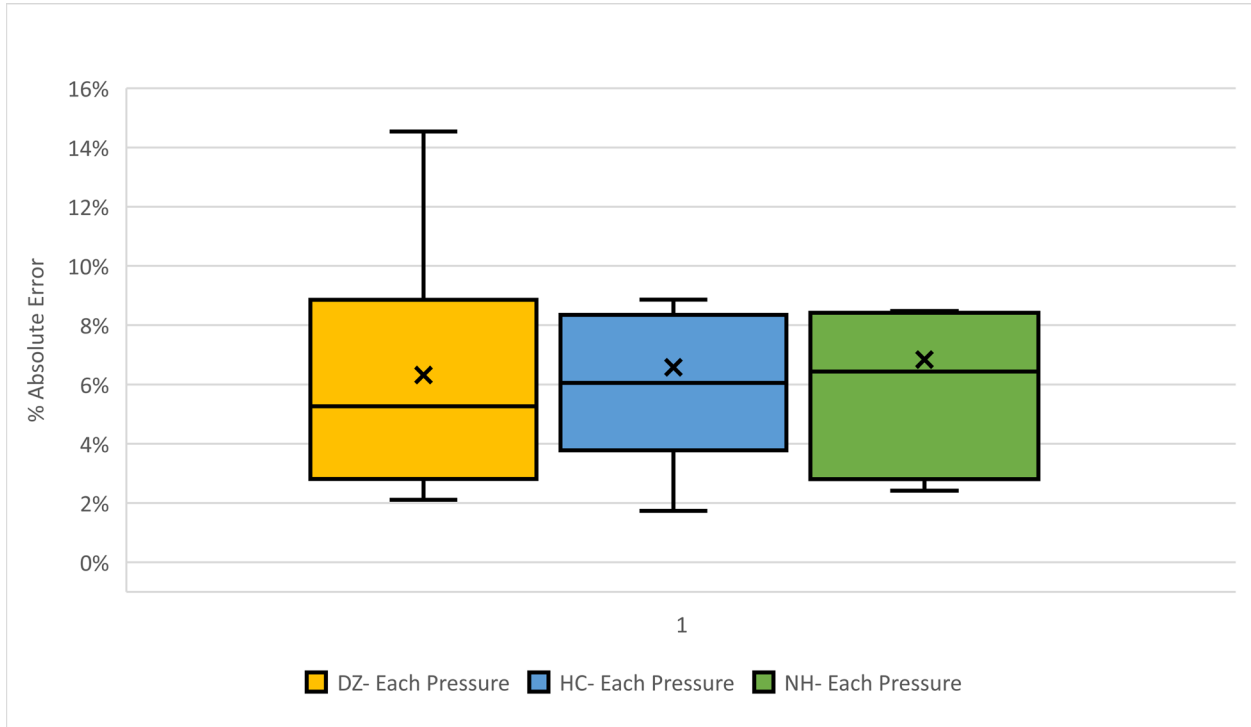


Figure C-2: Absolute Error Statistical Comparison for 3 Kinetic Methods from A_{30} values found using Each Pressure Group

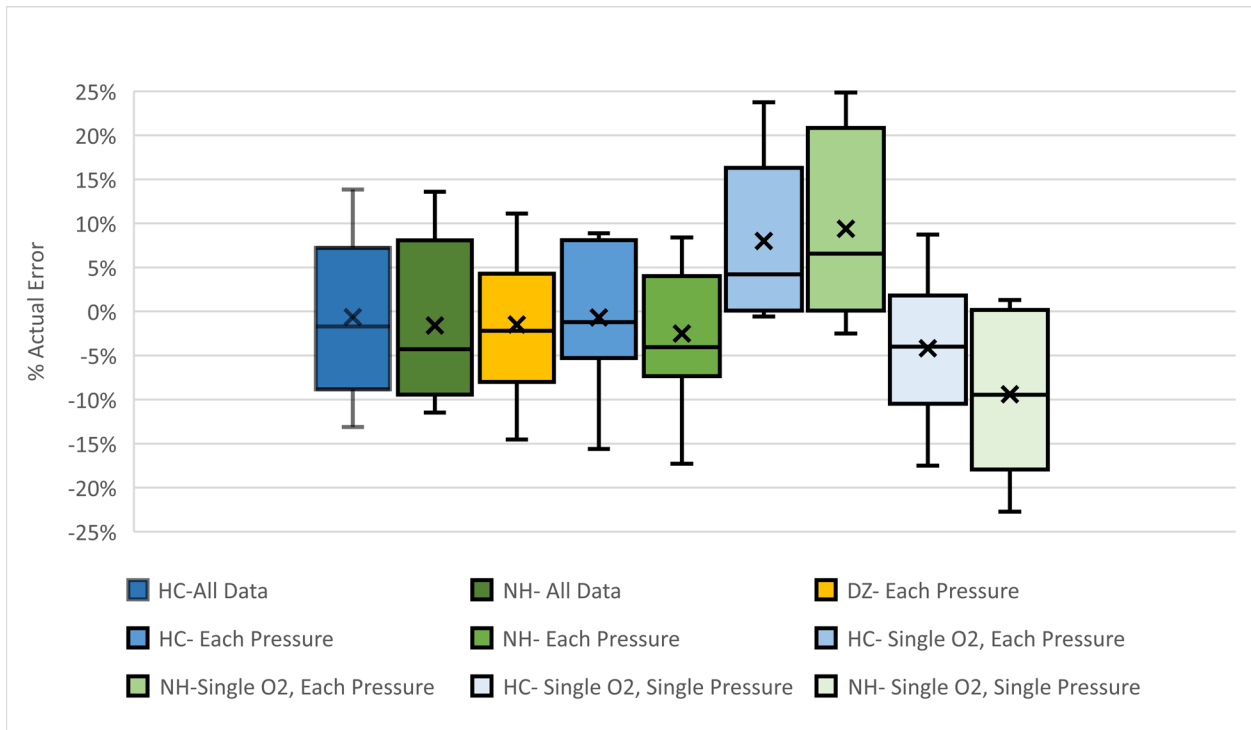


Figure C-3: Actual Error Statistical Comparison-All Modeling Methods

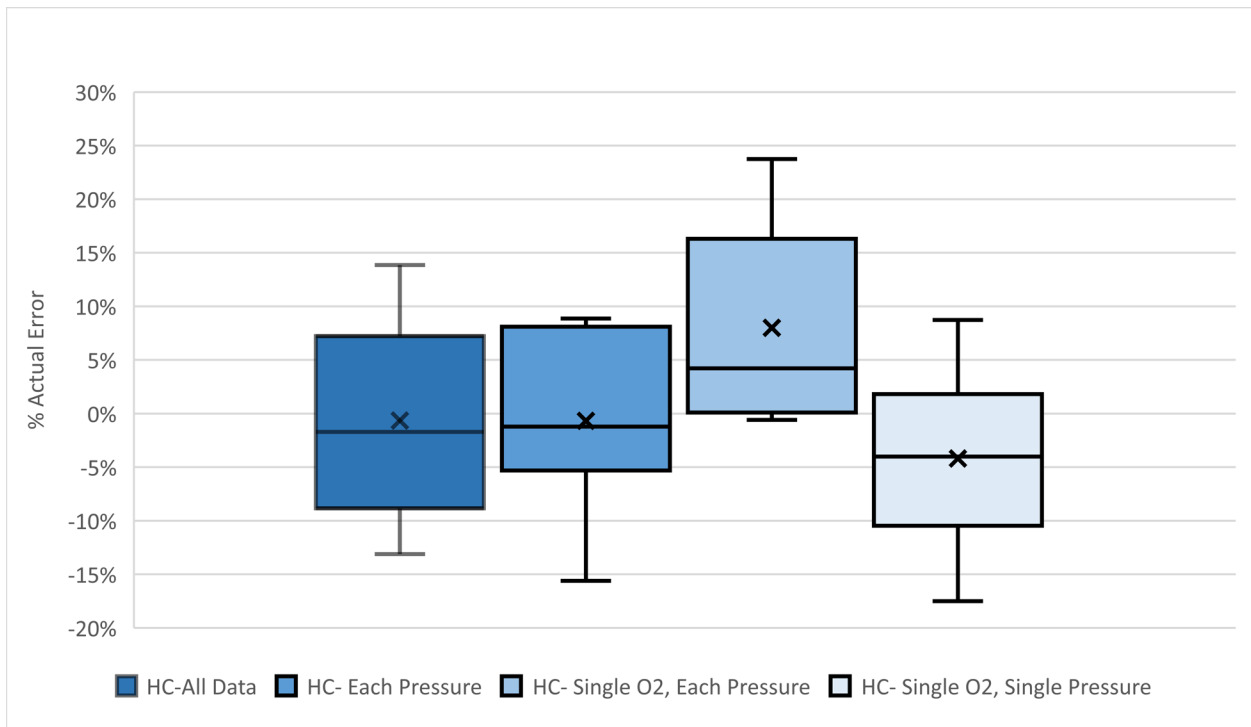


Figure C-4: Actual Error Statistical Comparison using all Hurt-Calo modeling

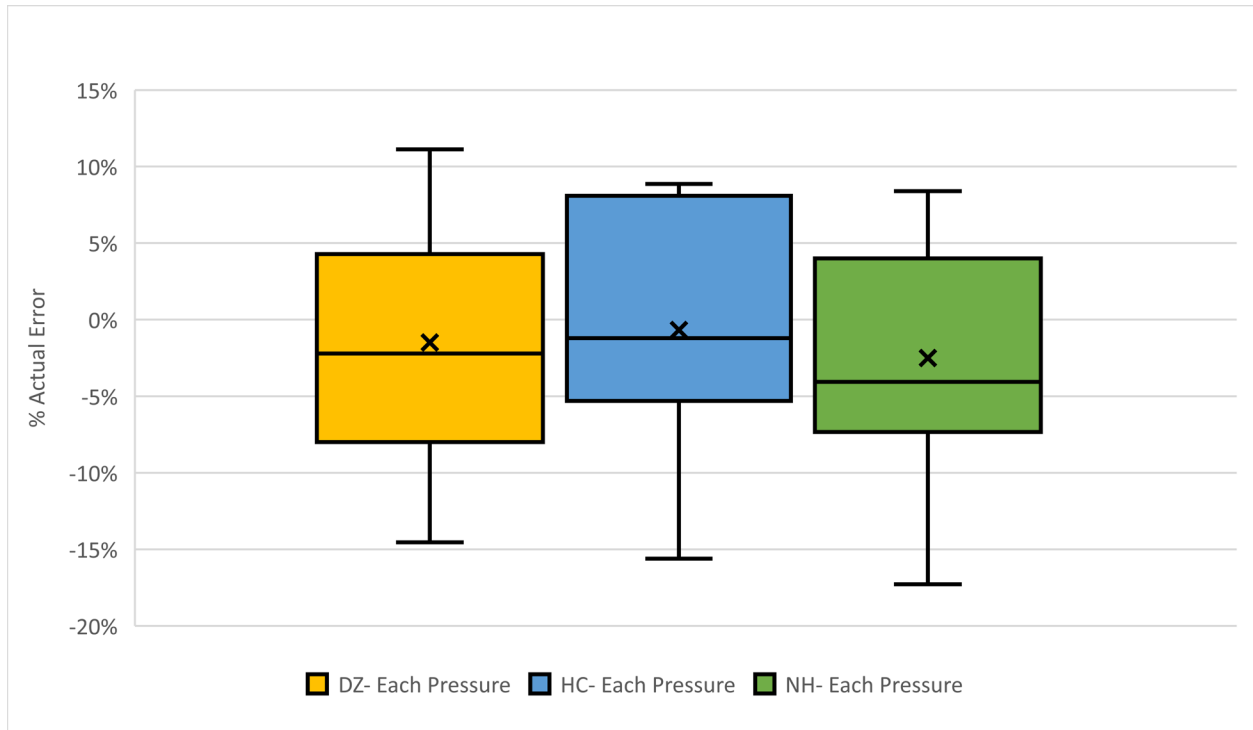


Figure C-5: Actual Error Statistical Comparison for 3 Kinetic Methods from A_{30} values found using Each Pressure Group

Table C-3: Pre-exponential Factors from Modeling (for single point solutions)

Pressure (atm)	Single O ₂ at a Pressure		Single O ₂ (5.12%) for a single Pressure (2.5 atm)	
	Hurt-Calo (sec ⁻¹)	Niksa-Hurt (sec ⁻¹)	Hurt-Calo (sec ⁻¹)	Niksa-Hurt (sec ⁻¹)
2.5	3.40×10^{18}	3.52×10^9	3.40×10^{18}	3.52×10^9
6	2.37×10^{19}	3.61×10^9		
10	2.06×10^{18}	2.33×10^{11}		